

Multi-state Models For Disease Histories Based On Longitudinal Data

Simon Wiegrebe^{*1,2}, Johannes Piller^{*1,3}, Mathias Gorski², Merle Behr⁴, Helmut Küchenhoff¹, Iris M. Heid², and Andreas Bender^{3,5}

¹*Statistical Consulting Unit StaBLab, Department of Statistics, LMU Munich, Munich, Germany.*

²*Department of Genetic Epidemiology, University of Regensburg, Regensburg, Germany.*

³*Munich Center for Machine Learning, LMU Munich, Munich, Germany.*

⁴*Faculty of Informatics and Data Science, University of Regensburg, Regensburg, Germany.*

⁵*Department of Statistics, LMU Munich, Munich, Germany.*

Abstract

Multi-stage disease histories derived from longitudinal data are becoming increasingly available as registry data and biobanks expand. Multi-state models are suitable to investigate transitions between different disease stages in presence of competing risks. In this context, however, their estimation is complicated by dependent left-truncation, multiple time scales, index event bias, and interval-censoring. In this work, we investigate the extension of piecewise exponential additive models (PAMs) to this setting and their applicability given the above challenges. In simulation studies we show that PAMs can handle dependent left-truncation and accommodate multiple time scales. Compared to a stratified single time scale model, a multiple time scales model is found to be less robust to the data generating process. We also quantify the extent of index event bias in multiple settings, demonstrating its dependence on the completeness of covariate adjustment. In general, PAMs recover baseline and fixed effects well in most settings, except for baseline hazards in interval-censored data. Finally, we apply our framework to estimate multi-state transition hazards and probabilities of chronic kidney disease (CKD) onset and progression in a UK Biobank dataset (n=142,667). We observe CKD progression risk to be highest for individuals with early CKD onset and to further increase over age. In addition, the well-known genetic variant rs77924615 in the *UMOD* locus is found to be associated with CKD onset hazards, but not with risk of further CKD progression.

*These authors contributed equally to this work.

Keywords: piecewise exponential additive models, multi-state models, multiple time scales, index event bias, interval-censoring, chronic kidney disease

1 Introduction

As the adoption of registry data expands [1, 2] and biobanks gain importance [3, 4, 5], multi-stage disease histories are increasingly becoming available for use in both clinical routine and epidemiological research. Examples include Chronic Kidney Disease (CKD), where disease stages are defined by thresholds of serum creatinine-based estimated glomerular filtration rate (eGFR) measurements [6]; diabetes, defined based on fasting plasma glucose levels [7]; or age-related macular degeneration (AMD), characterized by the accumulation of subretinal drusenoid deposits (early/intermediate AMD) and cell atrophy (late AMD).

In this context, it is usually of interest to study transitions and risk factors conditional on current disease stage: For example, given onset of Mild CKD at 50 years of age and progression to Severe CKD 10 years later, what is the probability of developing end-stage kidney disease (ESKD) within the next t years? And is a genetic variant a risk factor for CKD onset, for CKD progression, or for both? It is appealing to employ multi-state models [cf. 8, 9] to derive transition probabilities and risk factor associations of multi-stage disease histories, such as CKD stages (Figure 1).

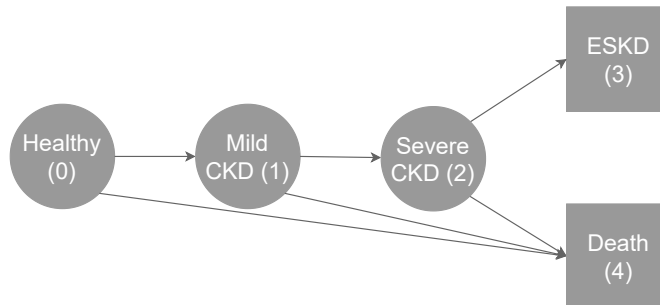


Figure 1: State diagram for Chronic Kidney Disease. This state diagram illustrates states and transitions within a chronic kidney disease (CKD) disease history. Circles represent transient states (Healthy (initial state), Mild CKD, Severe CKD), squares represent absorbing states (end-stage kidney disease (ESKD; considered to be absorbing here), Death). The arrows between states indicate possible/allowed transitions: $0 \rightarrow 1$ (CKD onset), $1 \rightarrow 2$ (progression to Severe CKD), $2 \rightarrow 3$ (progression to ESKD), as well as transitions into Death out of all transient states.

Multi-stage disease histories can be formalized as a stochastic process $(X_t)_{t \geq 0}$,

where X_t denotes the occupied state at time t from a finite state space $\mathcal{S} := \{0, 1, \dots, K\}$. As the process evolves over time, it induces a filtration $\mathcal{F}_t := \sigma(X_s : 0 \leq s \leq t, \mathbf{x})$, representing the information available up to time t . This filtration comprises the observed trajectory of the process on $[0, t)$ as well as covariates \mathbf{x} , which may be time-dependent but are assumed to be observed prior to time t .

Within this framework [cf. 8, 10, 11, 12], for states $o, \ell \in \mathcal{S}$ with $o \neq \ell$ and times $s, t \in [0, \tau)$ such that $s < t$, multi-stage disease histories are characterized by transition probabilities

$$p_{o\ell}(s, t) = \mathbb{P}(X_t = \ell \mid X_s = o, \mathcal{F}_s), \quad (1)$$

or, equivalently, by transition intensities

$$\alpha_{o\ell}(t) = \lim_{\Delta t \rightarrow 0} \frac{1}{\Delta t} p_{o\ell}(t, t + \Delta t). \quad (2)$$

Assuming Δt to be infinitesimally small and defining the probability to stay in state o as $\alpha_{oo}(t) = -\sum_{\ell \neq o} \alpha_{o\ell}(t)$, the empirical transition probability matrix $\mathbf{P}(s, t) = (p_{o\ell}(s, t))_{o, \ell \in \mathcal{S}}$ follows from the cumulative transition intensity $d\mathbf{\Lambda} = (\alpha_{o\ell}(t)\Delta t)_{o, \ell \in \mathcal{S}}$, and can be calculated via the product integral over time interval $[s, t)$ [13, 10], i.e.,

$$\mathbf{P}(s, t) = \prod_{u \in [s, t)} (\mathbf{I} + d\mathbf{\Lambda}(u)). \quad (3)$$

Oftentimes, $(X_t)_{t \geq 0}$ is assumed to be Markov, i.e., $\mathbb{P}(X_t = \ell \mid X_s = o, \mathcal{F}_s) = \mathbb{P}(X_t = \ell \mid X_s = o)$; in other words, the transition probability is assumed to solely depend on the past via the current time s and the occupied state. Traditional approaches to multi-state modeling, such as the non-parametric Aalen-Johansen (AJ) estimator [13] or cause-specific Cox Proportional Hazards (PH) models [14], have limited support for handling non-Markov scenarios and non-linear effect modeling. Within a Markov framework, recent Bayesian and continuous-time approaches have advanced the modeling of time-inhomogeneous disease progression [15, 16, 17]. However, these methods remain fundamentally limited by the Markov assumption, which precludes the incorporation of subject-level history-dependent information. Alternative semi-Markov approaches, such as the Bayesian accelerated failure time (AFT) model [18], have been developed to handle interval-censored data while relaxing restrictive Markov assumptions. However, these methods typically rely on parametric distribution families for transition times, which can entail severe bias in baseline hazard estimation if the underlying distribution is misspecified.

Furthermore, the application of multi-state models in the context of multi-stage disease histories comes with additional statistical challenges:

- (a) Independence between (history-dependent) state-entry times and events may be violated [19, 20, 21].
- (b) There exist multiple time scales, which are not all jointly identifiable in subpopulations due to the age-period-cohort problem [22].

- (c) Negative correlation between otherwise uncorrelated risk factors may be induced within subsets of diseased individuals, causing index event bias [23].
- (d) Disease histories derived from longitudinal data tend to be interval-censored as traits are only assessed at (ir-)regular follow-up times [24].

Here, we propose to use a novel multi-state modeling framework based on piecewise exponential additive models (PAMs) [25, 26]: Within this framework, multi-state data encodes transitions via tuples $(y_{i,k}^{entry}, y_{i,k}^{exit}, d_{i,k}, \mathbf{x}_{i,k})$, where $i \in \{1, \dots, n\}$ is the subject index, k refers to the transition from state o to ℓ (also noted as $o \rightarrow \ell$), $y_{i,k}^{entry}$ and $y_{i,k}^{exit}$ are risk set entry and exit times, due to either transitioning or censoring, $d_{i,k}$ is the transition-specific status indicator, and $\mathbf{x}_{i,k}$ is the subject- and transition-specific covariate vector [27]. Transition intensities $\alpha_{o\ell}(t)$ are then computed through transition-specific hazards $h_k(t | \mathbf{x}_{i,k})$ (see Equations (4), (5), and (7)). This permits flexible specification of covariate-dependent hazards, thereby inducing transition probabilities that vary with the underlying covariate structure [26]. By further including history-dependent information – such as state-entry times or multiple time scales – into the estimation of $h_k(t | \mathbf{x}_{i,k})$ through covariate adjustment, this PAM-based framework can explicitly handle non-Markov scenarios. Moreover, baseline hazards are estimated much more flexibly, without relying on distributional assumptions, yet still in a fully parametric fashion. Finally, the proposed framework allows for seamless incorporation of time-varying covariates as well as flexible estimation of their (time-varying) effects, for instance via penalized splines.

In this work, we demonstrate the scope of the above challenges and how the PAM-based framework can cope with them. Section 2 introduces terminology and describes the statistical challenges in detail. Section 3 introduces the modeling framework. Section 4 provides the setup and results of simulation studies investigating the properties of this modeling framework under the various challenges. In Section 5, we apply the framework to a UK Biobank dataset on CKD, estimating baseline hazards and transition probabilities as well as risk factor associations for CKD onset and progression. Section 6 concludes, discusses limitations and provides directions for future research.

2 Challenges in Disease History Analysis

We discuss four challenges that arise when applying multi-state modeling techniques to multi-stage disease histories: dependent left-truncation, choice of time scales, index event bias, and interval-censoring. The second and third challenges are not limited to time-to-event approaches. Only the last one is specific to disease histories derived from interval-structured longitudinal data.

2.1 Dependent left-truncation

The multi-state process induces left-truncation because subjects enter the risk set for transition k at different time points, i.e., at subject-specific state-entry times. For the above CKD example, a subject with CKD *onset* at age 50 years is only at risk of CKD *progression* after CKD onset and is thus left-truncated for CKD *progression* prior to the age of 50 (see subject B in Figure 2). An estimator for the transition-specific hazards $h_k(t \mid \mathbf{x}_{i,k})$ therefore needs to be able to take this into account. In general, left-truncation can be accounted for by non- and semi-parametric methods, provided that state-entry times (which represent the left-truncation times) can be assumed to be independent of event times. Such methods include the AJ estimator and the Cox PH model, which adjust the risk sets accordingly [8, 28].

However, state-entry times may not necessarily be independent of event times [19, 20, 21]: For instance, subjects with disease onset at a young age are possibly at higher risk of disease progression than subjects with late disease onset, implying dependence between truncation times and event occurrence. This dependence might not be linear on the log-hazard scale.

2.2 Choice of time scales

Hazards for all transitions of a multi-state model are commonly modeled on a single time scale, typically the natural time scale for transitions out of the initial state [22]. We call such a model with transition-specific stratification of the baseline hazard a *stratified single time scale* model. Risk sets for all transitions are defined along that single time scale t . Since the popular AJ estimator and Cox PH model can, by design, only incorporate a single time scale, the use of the *stratified single time scale* approach is further reinforced.

In general registry data, entry into the dataset is random and not linked to the start of disease or intervention. Then, the baseline time scale is typically chronological age [29, 30] and age at disease onset is the time-to-event for the transition from "healthy" into "diseased". For transitions into higher disease states or for clinical studies in patients (disease progression), the time since entry into the intermediate state is the relevant time scale [22, 31]. In clinical studies, time to recovery or relapse can be alternative time scales. This multiplicity of relevant time scales is illustrated for CKD onset and progression in Figure 2: For example, the hazard of progressing to Severe CKD for subject B at 57 years of age might depend not only on age, but also on time since CKD onset (i.e., 7 years). As a consequence, it may be of interest to allow transition intensities of a multi-state model to vary along multiple time scales; in the CKD example, the time scales are chronological age, time since CKD onset, and time since CKD progression. This way, baseline hazards can be captured by (a combination of) distinct time scales which commence at the time of entry into the different states [22, 32]. We call this the *multiple time scales* approach.

It is possible to jointly estimate the effects of multiple time scales and state-entry times by fitting one model on the entirety of disease trajectories, thus

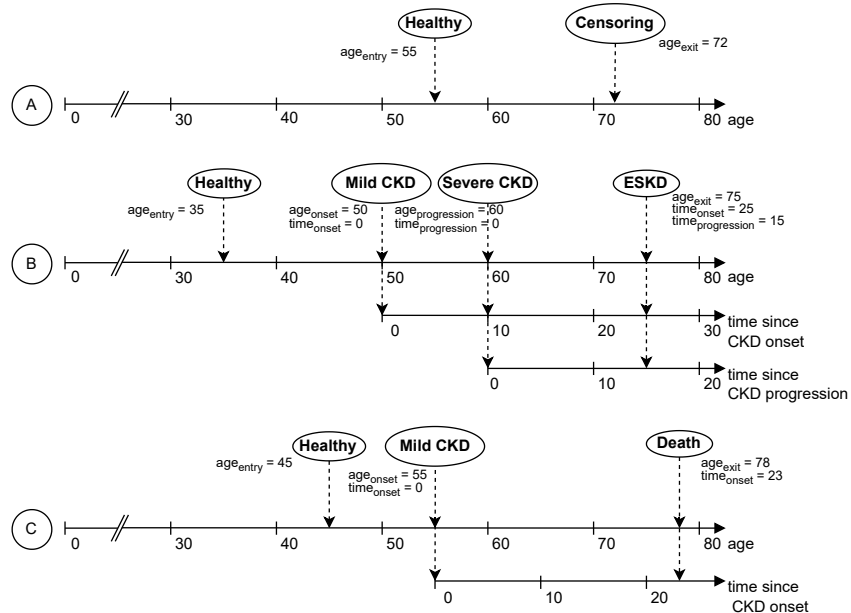


Figure 2: Examples of disease histories regarding CKD. Based on the state diagram in Figure 1, this figure illustrates CKD onset and progression histories of three hypothetical subjects. Commencing at study entry (Healthy), the disease histories terminate in the absorbing states ESKD or Death or cease to be observable following right-censoring. Horizontal arrows represent time scales. The precise definitions of time scales and state-entry times, as well as the practical implementation via transition-specific helper variables, are described in Section 3.

circumventing the identifiability problem of age-period-cohort models [22]. However, this requires fully parametric models with respect to parameter estimation, such as the piecewise exponential model [33] or discrete-time models [34]. The specific choice of (multiple) time scales can then be considered as an empirical – and thus, dataset-specific – question [22].

2.3 Index event bias

Diseases are typically multi-factorial, where risk factors can depend on each other [35]. Even if risk factors are independent in the healthy population, a negative correlation may be induced between them if analyses are restricted to subjects who have previously experienced a so-called index event whose occurrence is influenced by these risk factors. As an example, consider the index event CKD onset and two independent risk factors: the genetic variant rs77924615 from the *UMOD* locus (known to be associated with kidney function decline

[36, 31]) and diabetes. When studying risk factor associations with CKD progression and thus restricting to CKD patients, the genetic variant will likely be associated with absence of diabetes (and vice versa) because people with the genetic variant are less likely to require an additional risk factor in order to be in the CKD subgroup.

As a consequence, failing to include other (confounding) risk factors into an analysis restricted to such a subgroup causes biased estimation of the effect of the risk factor of interest, in the form of attenuation or even effect reversal. This particular form of selection bias is referred to as index event bias (IEB) [23].

Conditioning on index events is inherent to multi-state models, due to their conditional view: For transitions out of all non-initial states $\tilde{\ell} \neq 0$, we condition on having previously transitioned into $\tilde{\ell}$. As a consequence, we expect all risk factors to be affected by IEB for progression analysis. In addition, as omitted variable bias (OVB) is known to affect time-to-event approaches by biasing effect size estimates towards zero [37], we additionally expect OVB-driven attenuation for all states.

2.4 Interval-censoring

Longitudinal datasets are routinely obtained either from cohort studies with mostly prespecified examination times or from registry data with irregular and subject-specific visit numbers and times [38, 39, 40, 41, 42]. In both cases, we have a natural interval structure for each subject, implying that event times from longitudinal data are typically interval-censored [24].

The degree of interval-censoring (IC) inherently depends on interval lengths. For registry data, interval lengths tend to be smaller for less healthy individuals, who in turn are more prone to have events ("informative observation") [43, 44]. This, as well as the fact that the common endpoint Death (cf. Figure 1) is usually recorded precisely ["dual censoring"; 45, 46], limits the potential extent of IC.

3 Flexible Modeling of Disease Histories Using Piecewise Exponential Additive Models

We now introduce the piecewise exponential model (PEM) framework, a flexible approach for modeling disease histories, particularly in light of the challenges presented in Section 2.

PEMs [33] reduce survival tasks (based on right-censored, potentially left-truncated data) to standard Poisson regression tasks (of uncensored data) via transformation of the original survival data into a piecewise exponential data (PED) format (Appendix A.1.1). The piecewise exponential additive model (PAM) [47] is an extension of the PEM that estimates the baseline hazard as a smooth function over time, typically via penalized splines. This obviates the need for a specific choice of interval cut points while also making the estimation of baseline hazards more robust. Related approaches have been discussed in the

literature [48, 49, 50]. Given the PED format, model estimation of a PAM is thus analogous to that of a penalized additive Poisson regression, typically via Restricted Maximum Likelihood (REML) estimation [51, 52] and using standard software for the estimation of generalized additive models such as the R package `mgcv` [53]. For large datasets (e.g., the UK Biobank CKD dataset used in Section 5), significant gains in memory efficiency and computational speed can be achieved by using `mgcv::bam()` with fast Restricted Maximum Likelihood (fREML) and covariate discretization. The estimation techniques from single-event PEMS/PAMs can be directly applied to multi-state modeling, with the key difference that subjects can now enter and switch between different states. This, in turn, requires the PED to be further augmented (Appendix A.1.2).

In the following, we introduce two baseline multi-state PAMs: the *stratified single time scale (SSTS)* PAM, which estimates transition-specific baseline hazards along a single time scale, t ; and the *multiple time scales (MTS)* PAM, which expresses baseline hazards in terms of (combinations of) multiple time scales. These baseline models are subsequently extended to account for dependent left-truncation and to include covariates.

Single Stratified Time Scale PAM

The transition-specific baseline hazard of the *SSTS* PAM is

$$h_{0,k}^{ssts}(t) = \exp\left(\beta_{0,k} + f_k^{ssts}(t)\right), \quad (4)$$

where $\beta_{0,k}$ is a log-hazard baseline level and $f_k^{ssts}(t)$ is a smooth, possibly non-linear function of t , estimated via penalized splines (cf. Equation (11)). For estimation, we parameterize $f_k^{ssts}(t) = \sum_{m=1}^{M_k} \gamma_{m,k} B_{m,k}(t)$ with basis coefficients $\gamma_{m,k}$ and basis functions $B_{m,k}$ (e.g., B-splines or thin-plate splines). As the parameters of each function $f_k^{ssts}(t)$ are estimated independently of each other (with separate penalty terms), model (4) can be viewed as a smooth version of the AJ estimator.

Multiple Time Scales PAM

For a general definition of the baseline hazard of an *MTS* PAM, we consider progressive disease states $d \in \{0, \dots, D\}$ (0 being the initial (healthy) state and D the final, absorbing one). We further consider n_R (terminal) competing risks $R \in \{D+1, \dots, D+n_R\}$. For instance, in Figure 1 we have $D = 3$ and a single competing risk $R = 4$ ($n_R = 1$). In addition, we define:

- the set of all disease onset and progression transitions out of state d or higher states, $\mathcal{S}_{dD} := \{d \rightarrow d+1, \dots, D-1 \rightarrow D\}$ (in Figure 1 for $d = 0$: $\mathcal{S}_{03} = \{0 \rightarrow 1, 1 \rightarrow 2, 2 \rightarrow 3\}$);

- the set of all transitions into R out of state d or higher states, $\mathcal{S}_{dR} := \{d \rightarrow R, \dots, D-1 \rightarrow R\}$ (in Figure 1 for $d=0$: $\mathcal{S}_{04} = \{0 \rightarrow 4, 1 \rightarrow 4, 2 \rightarrow 4\}$);
- time scales t_d , representing the initial time scale for $d=0$ (identical to t in Equation (4)) or time since entry into state d for $d > 0$ (set to 0 for transitions out of states $\tilde{d} < d$; cf. Figure 2);
- the effect of time scale t_d on transitions in \mathcal{S}_{dD} , $f_{dD}(t_d)$;
- the effect of time scale t_d on transitions in \mathcal{S}_{dR} , $\tilde{f}_{dR}(t_d)$.

$\mathcal{S}_{0D} \cup (\bigcup_{R=D+1}^{n_R} \mathcal{S}_{0R})$ thus represents the set of all possible transitions. We distinguish between transitions in \mathcal{S}_{dD} versus \mathcal{S}_{dR} , because former ones characterize (consecutive) disease onset and progression transitions, whereas latter ones refer to direct transitions into a terminal (competing risk) state.

The baseline hazard of an *MTS* PAM for transition k out of state d_k is then

$$h_{0,k}^{mts}(\mathbf{t}_k) = \exp \left(\beta_{0,k} + \sum_{d=0}^{D-1} \left\{ \mathbb{1}_{\mathcal{S}_{dD}}(k) \cdot f_{dD}(t_d) + \sum_{R=D+1}^{D+n_R} \mathbb{1}_{\mathcal{S}_{dR}}(k) \cdot \tilde{f}_{dR}(t_d) \right\} \right), \quad (5)$$

where $\mathbf{t}_k = (t_0, \dots, t_{d_k})$ is the vector of relevant time scales for transition k . $\mathbb{1}_A(x)$ is the indicator function taking on the value 1 if $x \in A$ and 0 otherwise (cf. Equation (12)).

Accounting for dependent left-truncation and inclusion of covariates

As discussed in Section 2.1, left-truncation may not be independent of event occurrence. It is possible to account for this by incorporating state-entry times into the model [10, 54, 55]. While the exact state-entry time (e.g., the time of CKD onset) is interval-censored, its *detection* time point is known and can be considered an actual new state because treatment, follow-up frequency, etc. change upon *detection*. Since PAMs do not rely on the Markov assumption and can flexibly estimate covariate effects, state-entry times (as well as other history-dependent variables) can be directly included into the model, typically as spline-based smooth effects. The inclusion of state-entry times $\mathbf{x}_k^{entry} = (t_{entry-1}, \dots, t_{entry-d_k})$ into a multi-state PAM requires the exact same stratification procedure as required for additional time scales t_d of the *MTS* PAM, including setting $t_{entry-d} := 0$ for transitions out of states $\tilde{d} < d$.

When incorporating relevant state-entry times for transition k , \mathbf{x}_k^{entry} , in order to account for dependent left-truncation, the hazard becomes

$$h_{entry,k}^m(\mathbf{t}_k, \mathbf{x}_k^{entry}) = h_{0,k}^m(\mathbf{t}_k) \cdot \underbrace{\exp \left(\sum_{d=1}^{D-1} \left\{ \mathbb{1}_{\mathcal{S}_{dD}}(k) \cdot f_{entry-d}(t_{entry-d}) + \sum_{R=D+1}^{D+n_R} \mathbb{1}_{\mathcal{S}_{dR}}(k) \cdot \tilde{f}_{entry-d}(t_{entry-d}) \right\} \right)}_{\eta_k^{entry}}, \quad (6)$$

for $m \in \{ssts, mts\}$. (Note that for the *SSTS* PAM, $\mathbf{t}_k = t, \forall k$.) Importantly, state-entry times are defined as the transition time (or age) *into* another state, so they do not apply to the initial state. Consequently, the summation is restricted to non-initial transient states $d = 1, \dots, D - 1$. In Section 5.3.1 (in particular, in Figure A.14), we show the relevance of modeling such state-entry time effects flexibly.

The hazards of multi-state PAMs can be further expanded to include any other (time-varying or time-constant) covariates \mathbf{x}_k , yielding the general form

$$h_k^m(\mathbf{t}_k, \mathbf{x}_k^{\text{entry}}, \mathbf{x}_k) = h_{0,k}^m(\mathbf{t}_k) \cdot \exp\left(\eta_k^{\text{entry}} + g(\mathbf{x}_k, \mathbf{x}_k^{\text{entry}}, \mathbf{t}_k, k)\right). \quad (7)$$

Here, $g(\mathbf{x}_k, \mathbf{x}_k^{\text{entry}}, \mathbf{t}_k, k)$ is a potentially non-linear function representing the effects of covariates that may also interact with time scales, state-entry times, and transitions [25].

Identifiability of multi-state PAMs

In order to jointly estimate multiple time scales and state-entry times, it is necessary to fit a single model to the entirety of disease trajectories [22] (see Section 2.2). In this case, however, the implementation of multi-state models so as to ensure model identifiability is not straightforward. For the design matrix to be of full rank, effects of t_d and $t_{\text{entry},d}$ must only be estimated (and, e.g., spline bases set up) for those transitions where t_d and $t_{\text{entry},d}$ actually vary. Estimating such effects for transitions $\tilde{d} < d$ (where $t_d = t_{\text{entry},d} = 0$) introduces redundant (perfectly collinear) columns into the design matrix. This, in turn, results in rank-deficiency and loss of identifiability, in particular for transition main effects and the effects of t_d and $t_{\text{entry},d}$.

In Equations (5) and (6), transition-specific effects of multiple time scales and state-entry times are specified by means of the indicator functions $\mathbb{1}_{\mathcal{S}_{dD}}(k)$ and $\mathbb{1}_{\mathcal{S}_{dR}}(k)$. For practical implementation, we need to specify helper variables for all transient states $d \in \{0, \dots, D - 1\}$ in order to stratify the effects of t_d and $t_{\text{entry},d}$.

Due to the presence of multiple time scales, *MTS* PAMs always require the construction of such helper variables in order to stratify the effect of each t_d (and, potentially, $t_{\text{entry},d}$ and other history-dependent covariates) by all possible subsequent transitions, $d \rightarrow d + 1$ and $d \rightarrow R$, $R \in \{D + 1, \dots, D + n_R\}$. To this end, we define categorical variables $trans_{\text{after},d}$, which take on the value *progression* for all progression transitions out of states $d, \dots, D - 1$ and $d \rightarrow R$ for transition into terminal state R . In addition, for each non-initial transient state $d \in \{1, \dots, D - 1\}$, we set $trans_{\text{after},d}$ to the value *none* for transitions out of states $\tilde{d} < d$. This handles subjects who have not yet or never will transition into state d . We can then estimate the effects of all terms t_d and $t_{\text{entry},d}$, stratified by the subsequent transition, simultaneously, typically via spline-based smooth effects.

For *SSTS* PAMs, such helper variables are necessary in case state-entry times (or any other history-dependent covariates) are included into the model. In this case, the required helper variables $trans_{\text{after}_d.\text{exact}}$ are identical to the transition variable k for transitions out of states $\tilde{d} \geq d$, but take on the value *none* for transitions out of states $\tilde{d} < d$.

We present two approaches to resolve the issue of non-identifiability. The first approach consists in setting *none* as the reference level of the helper variables, so that no separate effect is estimated for the corresponding transitions. (For instance, in Figure 1, we do not wish to estimate the effect of t_1 (time since CKD onset) for transitions out of state 0.) For the `pamtools` implementation, which uses `mgcv::gam()` [53] in the background, this can be achieved by coding $trans_{\text{after}_d}$ and $trans_{\text{after}_d.\text{exact}}$ as *ordered* factor variables with reference level *none* and estimating t_d and t_{entry_d} as penalized splines. Then, `mgcv::gam()` only sets up basis functions for the non-reference levels of the helper variables, as desired.

The second approach removes the perfectly collinear design matrix columns (i.e., those where the helper variables are equal to *none*) through penalization. For the `pamtools` implementation, we can achieve this by using factor smooths (instead of penalized splines) to estimate the stratified t_d and t_{entry_d} effects (`mgcv` version 1.9-3) [53]. The factor smooth, which is actually a random effects-style smoother [56], only estimates a single, shared smoothing parameter λ across all levels of the helper variable, while penalizing all null space components and thus "penalizing away" the non-informative and perfectly collinear spline basis coefficients of those subjects where the helper variable is equal to *none*.

In the simulation study in Section 4.1, we test and contrast both of these two approaches to achieving identifiability.

4 Simulation studies

In this section, we present the setup and results of simulation studies investigating the impact of the challenges in Sections 2.2, 2.3, and 2.4. For this purpose, we design challenge-specific data generating processes (DGPs) and use different specifications of the PAM approach (Section 3) for estimation.

For all simulations, we employ a study time window of $t \in (0, 10]$ with administrative censoring at $t = 10$ and grid points $0.1, 0.2, \dots, 9.9, 10$ for evaluation. Note that for transitions $1 \rightarrow 2$ and $1 \rightarrow 3$ of the multi-state DGPs (Sections 4.1 and 4.2), the evaluation grid is two-dimensional: $t \in \{0, 0.1, \dots, 9.9, 10\}$ and $t_{\text{entry}_1} \in \{0, 0.1, \dots, t\}$, as the time at entry into state 1 must not exceed the total time since study entry. Penalized splines are fitted with $k = 20$ basis functions to allow for sufficient flexibility.

We are interested, throughout, in the estimation of baseline (log-)hazards, cumulative hazards, and transition (or survival) probabilities (cf. Equations (4), (5), and (3)); as well as of associations of covariates (e.g., risk factors) with (log-)hazards (cf. Equation (7)). We judge estimation quality through

coverage. Pointwise coverage is computed for all grid points t (or t -by- t_{entry_1}) by evaluating whether the true quantity of interest is covered by the corresponding estimated 95% confidence interval. Averaging across all simulation runs yields pointwise mean coverage and 95% confidence intervals, using an exact binomial test. For overall coverage, we subsequently average over all evaluation grid points.

We note that, by definition, results for log-hazards and hazards are identical in terms of coverage and directly proportional (up to exponentiation) in terms of scale. This is why we only report log-hazards in the figures and tables of this section.

4.1 Choice of time scales

We start by looking into how well an *SSTS* and an *MTS* PAM (Equations (4) and (5)) recover both baseline hazards and fixed effect hazards (e.g., of a risk factor) for the various transitions of a multi-state model. We consider the case of the estimated model being correctly specified – i.e., congruent with the DGP – and the case of misspecification.

4.1.1 Setup

We assume a state diagram with initial state 0, interim state 1, and absorbing states 2 and 3 ($k \in \{0 \rightarrow 1, 0 \rightarrow 3, 1 \rightarrow 2, 1 \rightarrow 3\}$); see Figure 3. In terms of complexity, this state diagram ranks between a standard Illness-Death model and the model depicted in Figure 1, allowing us to study onset and progression dynamics (transitions $0 \rightarrow 1$ and $1 \rightarrow 2$, respectively) in the presence of a competing risk (3).



Figure 3: State diagram for simulation studies. This state diagram has initial state 0, interim state 1, and absorbing states 2 and 3. Arrows depict possible transitions: $0 \rightarrow 1$ (*onset*), $0 \rightarrow 3$ (*death without disease*), $1 \rightarrow 2$ (*progression*), and $1 \rightarrow 3$ (*death with disease*).

We consider two DGPs: First, the *SSTS* DGP assumes a single time scale t (cf. Equation (4)) and is characterized by the baseline hazard

$$h_{0,k}^{ssts}(t) = \exp\left(\beta_{0,k} + f_k^{ssts}(t)\right). \quad (8)$$

Second, the *MTS* DGP assumes the existence of one baseline hazard over time t (i.e., the first time scale) for subjects with a disease transition ($0 \rightarrow 1$ or $1 \rightarrow 2$) and a distinct baseline hazard over t for subjects with a death transition ($0 \rightarrow 3$ or $1 \rightarrow 3$). Additionally, the *MTS* DGP assumes the existence of another baseline hazard over t_1 (time since entry into state 1, the second time scale) for those individuals with disease onset. This t_1 effect again differs between subjects with disease progression ($1 \rightarrow 2$) and subjects with death transition ($1 \rightarrow 3$). The baseline hazard of the *MTS* DGP is thus

$$\begin{aligned} h_{0,k}^{mts}(\mathbf{t}_k) &= \exp\left(\beta_{0,k} + \sum_{d=0}^{D-1} \left\{ \mathbb{1}_{\mathcal{S}_{dD}}(k) \cdot f_{dD}(t_d) + \sum_{R=D+1}^{D+n_R} \mathbb{1}_{\mathcal{S}_{dR}}(k) \cdot \tilde{f}_{dR}(t_d) \right\}\right) \\ &= \exp\left(\beta_{0,k} + \mathbb{1}_{\{0 \rightarrow 1, 1 \rightarrow 2\}}(k) \cdot f_{02}^{mts}(t) + \mathbb{1}_{\{0 \rightarrow 3, 1 \rightarrow 3\}}(k) \cdot \tilde{f}_{03}^{mts}(t) \right. \\ &\quad \left. + \mathbb{1}_{\{1 \rightarrow 2\}}(k) \cdot f_{12}^{mts}(t_1) + \mathbb{1}_{\{1 \rightarrow 3\}}(k) \cdot \tilde{f}_{13}^{mts}(t_1)\right), \end{aligned} \quad (9)$$

with possible from-states $d_k \in \{0, 1\}$ and corresponding vectors of relevant time scales $\mathbf{t}_k = (t_0)$ or (t_0, t_1) for $d_k = 0$ or 1 , respectively; $D = 2$ and $R = 3$; $\mathcal{S}_{dD} := \{0 \rightarrow 1, 1 \rightarrow 2\}$ and $\mathcal{S}_{dR} := \{0 \rightarrow 3, 1 \rightarrow 3\}$ for $d = 0$; $\mathcal{S}_{dD} := \{1 \rightarrow 2\}$ and $\mathcal{S}_{dR} := \{1 \rightarrow 3\}$ for $d = 1$.

For both DGPs, we assume the hazards of transitions after disease onset to be affected by the time of entry into state 1, $t_{\text{entry},1}$, again separately for subjects with disease progression and death transition. Whenever we wish to investigate the coverage of fixed effects, we additionally include a Bernoulli(0.5)-distributed covariate x_1 with transition-specific fixed effects $\beta_{x_1,k}$ on the log-hazard into the respective DGP. The DGP hazard then becomes

$$\begin{aligned} h_k^m(\mathbf{t}_k, t_{\text{entry},1}) &= h_{0k}^m(\mathbf{t}_k) \cdot \exp\left(\beta_{x_1,k} + \right. \\ &\quad \left. \mathbb{1}_{\{1 \rightarrow 2\}}(k) \cdot f_{\text{entry},1}(t_{\text{entry},1}) + \mathbb{1}_{\{1 \rightarrow 3\}}(k) \cdot \tilde{f}_{\text{entry},1}(t_{\text{entry},1})\right). \end{aligned} \quad (10)$$

for $m \in \{ssts, mts\}$. Detailed specifications of the transition-specific log-hazard functions and fixed effect parameters can be found in Table A.1.

For a given DGP, we simulate datasets of size $n = 5,000$ for a total of 500 simulation runs. For each dataset, we then draw transition times for each subject from a piecewise exponential distribution using the transition-specific log-hazards. We add random right-censoring to the simulated data by drawing censoring times c_i from a Weibull distribution with shape parameter $\sigma = 1.5$ and scale parameter $\lambda = 10$. We round event and censoring times to two decimals.

We fit both an *SSTS* PAM and an *MTS* PAM, specified using Equations (4) and (5), to the data generated from the two DGPs. In line with Sections 2.1 and 3, we adjust both models for dependent left-truncation by including state-entry time t_{entry_1} in the model (cf. Equation (6)). We estimate both t_1 and t_{entry_1} either via penalized splines or factor smooths. Whenever the DGP also contains a fixed effect, we include x_1 and its interaction with transition into the model (cf. Equation (7)).

We are interested in the estimation of baseline (log-)hazards, cumulative hazards, and transition probabilities, as well as of fixed effect hazards, for the different transitions and DGP-by-model-by-smooth scenarios.

4.1.2 Results

We find that baseline hazards for all transitions are recovered very well by the *SSTS* PAM, regardless of DGP (Table A.2). For the *MTS* PAM, coverage is nominal (i.e., 95%) in case of correct model specification; in case of misspecification, however, mean coverage of (log-)hazards drops as low as 69% (Table A.2). For transitions $0 \rightarrow 1$ and $0 \rightarrow 3$, this is due to overestimation of the hazard especially at later time points (Figure A.1), leading to a sharp increase in bias and root mean squared error (RMSE; Figure A.2). The choice of the smooth (penalized splines versus factor smooth) has little effect on baseline hazard coverage. The choice of the quantity of interest, on the other hand, is relevant: Coverage is generally higher for cumulative hazards and transition probabilities than for (log-)hazards. This is because, as hazards are aggregated over time, up- and downward biases cancel each other out (Table A.2).

When including a fixed effect into the DGP, both PAMs – regardless of DGP and smooth types – achieve (close to) nominal fixed effect coverage for all transitions (Figure 4, Table A.3).

4.2 Index event bias

4.2.1 Setup

For the simulations on the quantification of IEB when applying multi-state PAMs, we use the same simulation setup (state diagram, DGPs, models) as in the above simulations, except that we now extend the DGPs by adding two independent covariates: a risk factor of interest x_1 and another, potentially omitted risk factor x_2 . The risk factors are assumed to be either Bernoulli(0.5)- or $N(0, 1)$ -distributed. We consider small, medium and large effect size scenarios (Table A.4).

We first evaluate the correlation between the two risk factors in each non-absorbing state. As the two risk factors are independent in the healthy population (state 0) by design, we expect zero correlation in state 0 and a negative correlation in state 1, in line with IEB theory. Second, we evaluate the estimated effects of the risk factor of interest, x_1 , on onset and progression log-hazards when only x_1 is included in the model (and x_2 is omitted).

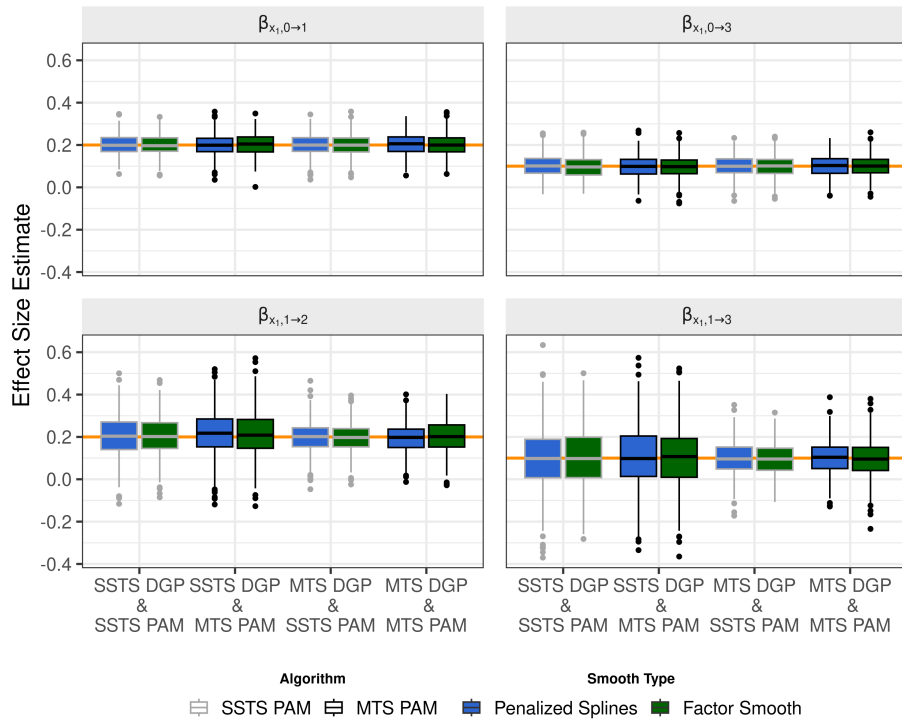


Figure 4: Fixed effect estimates by transition from *SSTS* and *MTS* PAMs on data simulated from *SSTS* and *MTS* DGPs. This figure illustrates first quartile, median and third quartile (boxes) of effect size estimates of a binary covariate x_1 on log-hazards across 500 simulation runs for transitions $k \in \{0 \rightarrow 1, 0 \rightarrow 3, 1 \rightarrow 2, 1 \rightarrow 3\}$. This is shown for *SSTS* and *MTS* PAMs, *SSTS* and *MTS* DGPs, and smooth types penalized splines versus factor smooth. Whiskers represent 1.5 times the interquartile range from the first and third quartile. Orange lines denote true effect sizes $\beta_{x_1,k}$.

We contrast this with the risk factor estimates after inclusion of x_2 into the model, which is expected to remove any bias.

4.2.2 Results

We observe correlation between x_1 and x_2 close to zero in state 0 across all risk factor distributions and effect size specifications, as expected (Figure 5a, Table A.5). In state 1, we observe negative correlation between the risk factors that becomes more pronounced as risk factor effect sizes increase.

We find little to no bias in settings where risk factor effect sizes are small, even in state 1 with a small induced negative correlation.

When considering large risk factor effect sizes, we find that the model including only x_1 yields biased effect estimates for both onset and progression

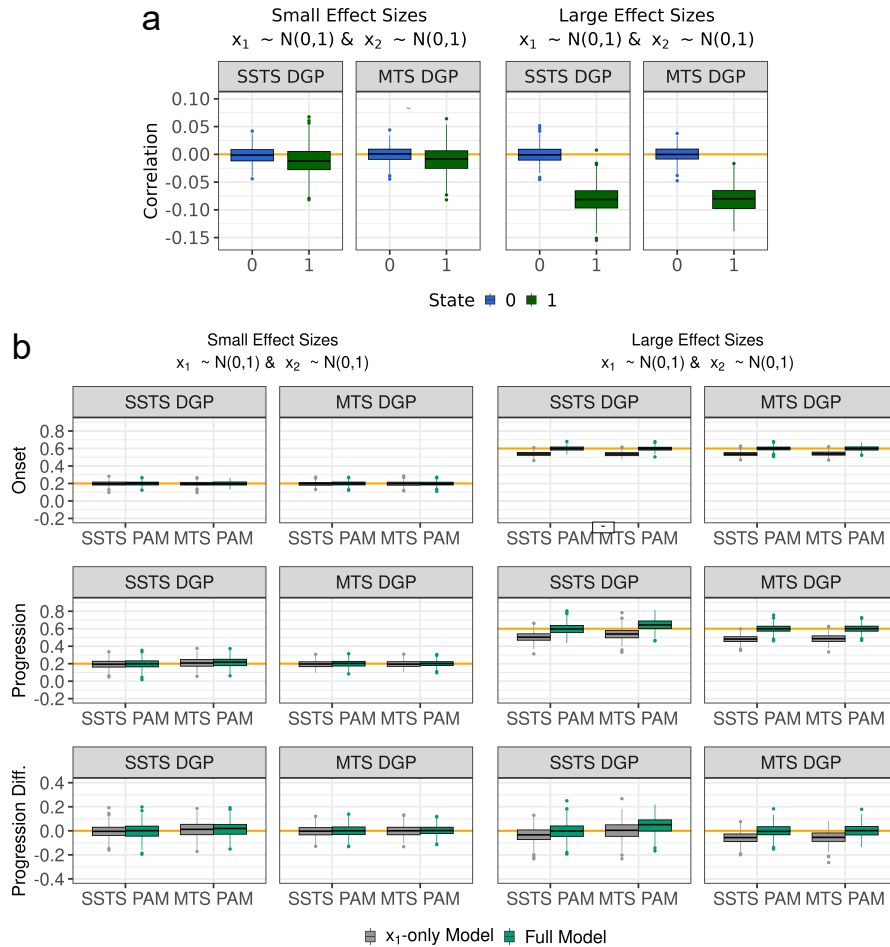


Figure 5: Induced negative correlation between risk factors and bias in effect size estimates in simulated multi-state data. Panel a shows Pearson correlation coefficients between two risk factors x_1 and x_2 in states 0 and 1, simulated as independent risk factors in the healthy population under *SSTS* and *MTS* DGPs. Panel b shows effect size estimates of risk factor x_1 on the log-hazards of disease onset ($\hat{\beta}_{x_1,0 \rightarrow 1}$; first row), disease progression ($\hat{\beta}_{x_1,1 \rightarrow 2}$; second row), and their respective difference (third row). The underlying data are again simulated from *SSTS* and *MTS* DGPs and analyzed with *SSTS* and *MTS* PAMs. The first (x_1 -only) model includes only the risk factor of interest, whereas the second (full) model includes both risk factors. Orange lines denote true effect sizes. The full table of results on correlations, effect size estimates, and bias for all DGPs, models, risk factor distributions, and risk factor effect sizes is available at <https://github.com/survival-org/msm4diseaseHistories>.

log-hazards: For two $N(0, 1)$ -distributed risk factors with large effect sizes, we observe mean estimated onset and progression effects as low as 0.54 and 0.48, respectively. This is a relative bias of 10% and 20%, given the true risk factor associations with onset and progression, $\beta_{1,onset} = \beta_{1,progression} = 0.6$ (Figure 5b). While the bias on $\beta_{1,onset}$ is OVB, the bias on $\beta_{1,progression}$ is attributable to both OVB and IEB. When including both risk factors x_1 and x_2 into the model, the bias is removed in all scenarios.

We find no difference in the bias between *SSTS* and *MTS* PAMs - regardless of the DGPs. This highlights, again, the relatively little importance of the choice of time scales when it comes to the estimation of fixed effect (i.e., risk factor) hazards.

4.3 Interval-censoring

In this section, we present a simulation study on the impact of IC on the estimation of fixed effect hazards as well as baseline (log-)hazards, cumulative hazards and survival probabilities. In doing so, we evaluate multiple DGPs, IC mechanisms, models, and estimation points.

4.3.1 Setup

To limit complexity, we here restrict to two states with one transition ($0 \rightarrow 1$), which reflects a standard survival setting. However, owing to the composite nature of multi-state models, these results directly carry over to more complex models, as in Sections 4.1, 4.2, and 5.

We consider the following three DGPs for the analysis of baseline hazard estimation under IC:

- a piecewise exponential DGP with baseline log-hazard of $-3.5 + 6 * f_0(t)$, where $f_0(t)$ is the density of a Gamma distribution with shape $\alpha = 8$ and scale $\sigma = 0.5$;
- a Weibull DGP with shape $\sigma = 1.5$ and log-hazard intercept $\beta_0 = -3.5$;
- and a Weibull-based DGP as implemented in the `simIC_weib()` function from the R package `icenReg` [57], with shape $\sigma = 1.5$ and scale $\lambda = 2$.

For the piecewise exponential and Weibull DGPs, we consider beta-distributed, uniformly-jittered, and equidistant observation times with 1 – 10 visit times per subject as IC mechanisms. The `icenReg`-based DGP employs a single uniform renewal IC mechanism.

Since here we have standard survival data and only a single transition type ($0 \rightarrow 1$), we can benchmark the performance of PAMs under IC by considering a total of four models:

- PAM (estimating the baseline hazard using penalized splines with $k = 20$ basis functions);

- Cox PH regression (not applicable for estimating baseline (log-)hazard rates; equivalent to the Nelson-Aalen estimator [58] and the Breslow estimator [59] for baseline cumulative hazards and the survival function, respectively, in the absence of covariates);
- and two AFT models (Weibull and Generalized Gamma).

For each of these models, we consider interval mid- and end-points as well as the exact time points (i.e., no IC) as estimation points. For AFT models, we additionally consider IC adjustment (i.e., direct incorporation of IC into the likelihood by considering both interval start and end point).

To evaluate the impact of IC on the estimation of fixed effect hazards, we add a Bernoulli(0.5)-distributed covariate x_1 to the log-hazard of the DGPs and the models, analogously to Section 4.1. In this case, we do not consider the `icenReg`-based DGP (incorporation of covariates with a pre-specified fixed effect on log-hazards not possible) nor the Generalized Gamma AFT model (not a PH model).

4.3.2 Results

The fixed effect of covariate x_1 on the log-hazard under IC is estimated correctly across all DGPs, IC mechanisms, models, and estimation points (Figure 6). The estimation bias is negligible, with coverage at the nominal level (Tables A.9 and A.10).

The mean coverage of baseline (log-)hazards by PAMs with interval mid-point estimation is between 50% and 75%, depending on specifications. PAMs with interval end-point perform consistently worse, due to a consistent time shift bias (Figure A.3). The high coverage of PAMs estimated using exact time points (no IC) underlines the model’s flexibility. The Weibull and Generalized Gamma AFT models achieve nominal coverage of baseline (log-)hazards whenever the DGP is Weibull-based and IC adjustment is employed - as expected. However, at the same time, their coverage is extremely low whenever the true DGP is not Weibull-based – which highlights these models’ limited flexibility in terms of estimating diverse baseline hazard shapes (Figure A.4, Table A.6).

For the piecewise exponential DGP, the coverage of baseline cumulative hazards and survival functions by PAMs is much higher, between 85% and 97%, depending on specifications. For the piecewise exponential DGP, the Weibull AFT model is, by far, the worst, due to its limited flexibility; the performance of the more flexible generalized Gamma AFT model is on par with that of the Cox model (which here defaults to the Nelson-Aalen estimator). For the Weibull DGP, the two AFT models with IC adjustment achieve nominal coverage (as expected), as does the PAM but not the Cox model (Figures A.5 and A.6, Tables A.7 and A.8).

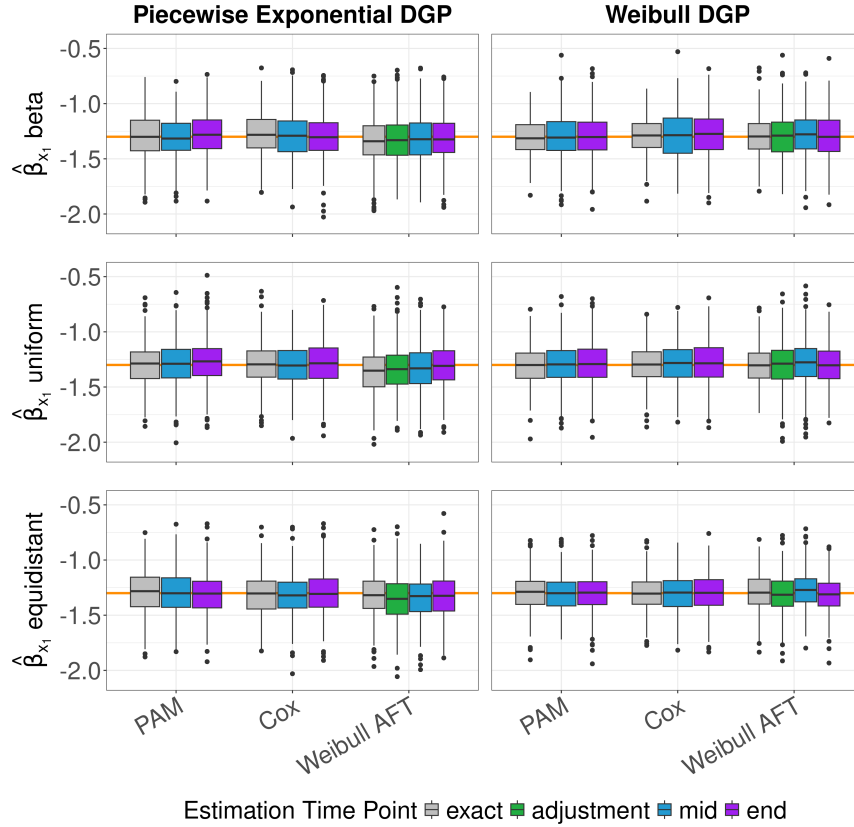


Figure 6: Boxplots of fixed effect estimates under interval-censoring. This figure shows boxplots of the estimated effect sizes of a *Bernoulli*(0.5)-distributed covariate on the log-hazard. Based on the simulation setup described in Section 4.3.1, effect sizes are estimated using three models (x-axis) and three to four distinct estimation points (color coding), on data generated by two DGPs (columns) and three IC mechanisms (rows). The orange line denotes the true effect on the log-hazard (-1.3).

5 Application: CKD Onset and Progression in UK Biobank

In this section, we study hazards, transition probabilities, and risk factors of CKD onset and progression (cf. Figure 1) in a large-scale UK Biobank (UKB) dataset [60]. Previous work on the same dataset has found the genetic variant rs77924615 (located in the *UMOD* locus, well known for association with CKD [61]) to be associated with kidney function decline over age and with CKD onset [31].

The multi-state approach presented here, which uses CKD stages instead of quantitative eGFR values, enables us to explicitly focus on CKD onset and progression of patients, as subjects who never get CKD – the large majority [31] – are considered to be censored (Table 1).

5.1 UK Biobank data on history of CKD stages

The UKB dataset curated by Gorski et al. [60] contains 2,080,372 eGFR measurements from $n = 454,071$ subjects, collected from serum creatinine measurements from blood drawn at two study center assessments as well as from electronic health records (eHRs). We include unrelated UKB participants of European ancestry (in line with Wiegrebe et al. [31]) with available eHR data. We exclude eGFR measurements at age < 35 years as well as between six months before and after acute kidney injury and nephrectomy, as in Wiegrebe et al. [31].

We apply KDIGO definitions [6] to define CKD stages: Healthy (eGFR ≥ 60 mL/min/1.73m²), Mild CKD (eGFR $\in [30, 60)$ mL/min/1.73m²), Severe CKD (eGFR $\in [15, 30)$ mL/min/1.73m²), and ESKD (eGFR < 15 mL/min/1.73m² or dialysis or kidney transplant). Healthy, Mild and Severe CKD are transient events, while both ESKD and Death are absorbing (see Figure 1); the Death state is defined based on available death registries linked to the UK Biobank, which provide the exact date of death (along with primary and contributory causes) according to the ICD-10 system.

To account for natural fluctuations when measuring eGFR, we require two subsequent eGFR measurements to fall below the respective transition thresholds for transitions into Mild and Severe CKD. For computational reasons, we round subject age to years. We impute missing interim CKD stages for "jump" transitions ($0 \rightarrow 2$, $0 \rightarrow 3$, and $1 \rightarrow 3$) – which in the case of CKD are due to interval-censoring and not to some separate transition mechanism – by linearly interpolating eGFR values. (This only applies to 213 subjects.)

The final multi-state dataset contains 142,667 subjects and 19,293 non-censoring transitions (Table 1).

5.2 Model specification

We draw on the conclusions from Section 4 to specify an *SSTS* and an *MTS* PAM with interval mid-point as estimation point. Here, we choose chronological *age* to be the primary time scale due to the non-informativeness of the study entry time point [31]. The baseline hazard model equation of the *SSTS* PAM for transitions k (cf. Figure 1; Equation (4)) is

$$h_{0,k}^{ssts}(age) = \exp\left(\beta_{0,k} + f_k^{ssts}(age)\right). \quad (11)$$

Table 1: Baseline characteristics and state transitions in the UKB dataset.

Characteristic	UKB Dataset (n = 142,667)
<i>Baseline Characteristics</i>	
Women, n (%)	76,705 (53.8)
Age at study entry	56.0 (35.0–77.0)
Age at study exit	65.0 (37.0–80.0)
<hr/>	
<i>Event Counts Overall</i>	
Transitions (incl. censoring)	148,757
Transitions (excl. censoring)	19,293
CKD-related transitions	6,660
Death transitions	12,633
<hr/>	
<i>Event Counts by Transition</i>	
Healthy →Mild CKD	6,079
Mild CKD →Severe CKD	436
Severe CKD →ESKD	145
Healthy →Death	11,153
Mild CKD →Death	1,351
Severe CKD →Death	129
<hr/>	
<i>Censoring</i>	
Censoring from Healthy	124,868
Censoring from Mild CKD	4,457
Censoring from Severe CKD	139
<hr/>	
<i>Interval Length by From-State*</i>	
Overall	1.44 (0.00–20.50)
Healthy	1.46 (0.00–20.50)
Mild CKD	0.68 (0.00–18.90)
Severe CKD	0.27 (0.00–5.64)

Ages and interval lengths are reported in years, as median (minimum–maximum).

CKD: Chronic Kidney Disease; ESKD: End-Stage Kidney Disease.

*Interval length: time between subsequent visits, i.e., evaluations of CKD stage.

For the *MTS* PAM, the baseline hazard model equation (cf. Equation (5)) is

$$\begin{aligned}
 h_{0,k}^{mts}(age, t_1, t_2) = \exp \left(\beta_{0,k} + \mathbb{1}_{\{0 \rightarrow 1, 1 \rightarrow 2, 2 \rightarrow 3\}}(k) \cdot f_{03}^{mts}(age) + \right. \\
 \mathbb{1}_{\{0 \rightarrow 4, 1 \rightarrow 4, 2 \rightarrow 4\}}(k) \cdot \tilde{f}_{04}^{mts}(age) + \\
 \mathbb{1}_{\{1 \rightarrow 2, 2 \rightarrow 3\}}(k) \cdot f_{13}^{mts}(t_1) + \mathbb{1}_{\{1 \rightarrow 4, 2 \rightarrow 4\}}(k) \cdot \tilde{f}_{14}^{mts}(t_1) + \\
 \left. \mathbb{1}_{\{2 \rightarrow 3\}}(k) \cdot f_{23}^{mts}(t_2) + \mathbb{1}_{\{2 \rightarrow 4\}}(k) \cdot \tilde{f}_{24}^{mts}(t_2) \right), \tag{12}
 \end{aligned}$$

where t_1 (time since onset of Mild CKD) and t_2 (time since progression to Severe CKD) are additional time scales (see Figure 2).

To adjust for dependent left-truncation, we include the two relevant state-entry times: age_1 (age at onset of Mild CKD) and age_2 (age at progression to Severe CKD); cf. Equation (6).

The stratification helper variables required for model identifiability, as defined in Section 3, are $trans_{after_1_exact}$ and $trans_{after_2_exact}$ for the *SSTS* PAM; and $trans_{after_0}$, $trans_{after_1}$, and $trans_{after_2}$ for the *MTS* PAM.

For IEB-related analyses (Section 5.3.2), we include the following risk factors in the model (stratified by transition; cf. Equation (7)): (i) the genetic variant rs77924615 (effect allele G); (ii) sex; (iii) a polygenic risk score (PGS) to control for other genetic variants associated with kidney function [62, 31]; (iv) binary diabetes and smoking status; and (v) body mass index (BMI) and urine albumin-to-creatinine ratio (uACR), both from UKB study center visits only.

All risk factors, except genetics and sex, are time-varying. The effects of time scales (age , t_1 , t_2), state-entry times (age_1 , age_2), and quantitative risk factors (PGS, BMI, uACR) are estimated via penalized splines ($k = 20$).

5.3 Results

5.3.1 Estimation of baseline hazards and state-entry times

First, we find that goodness of fit is better for the baseline *SSTS* PAM than for the baseline *MTS* PAM according to the Akaike Information Criterion (202, 412 versus 202, 445). This is in line with results from our simulations (Section 4.1.2) regarding the robustness of the *SSTS* PAM even under model misspecification.

Second, we consider estimated log-hazards and transition probabilities (Figures 7a-c and A.7-A.13). *SSTS* and *MTS* PAMs mostly produce similar estimates of baseline log-hazards and transition probabilities.

Log-hazards for the transition "Healthy \rightarrow Mild CKD" start increasing at age 40 years, further accelerate from age 60 on, and plateau at around age 75. The corresponding transition probabilities are close to zero until age 50, then increase. For the transition "Healthy \rightarrow Death", log-hazards rise steeply up to age 50, then almost plateau until almost age 65, followed by another increase thereafter. The corresponding direct transition probabilities increase exponentially, starting at age 50.

For transitions out of Mild CKD, evaluation does not only depend on the single time dimension of chronological age , but also on age_1 (age at onset of Mild CKD) and/or t_1 (time since onset of Mild CKD), with $age = age_1 + t_1$; see subjects B and C of 2 with $age_1 = age_{onset}$ and $t_1 = time_{onset}$. The "Mild CKD \rightarrow Severe CKD" transition probabilities are highest for subjects with early CKD onset (i.e., small age_1) and, for a given age_1 , increase over age . Direct "Mild CKD \rightarrow Death" transition probabilities again increase sharply with age (starting at around 50), independently of age_1 (Figures A.8 and A.9).

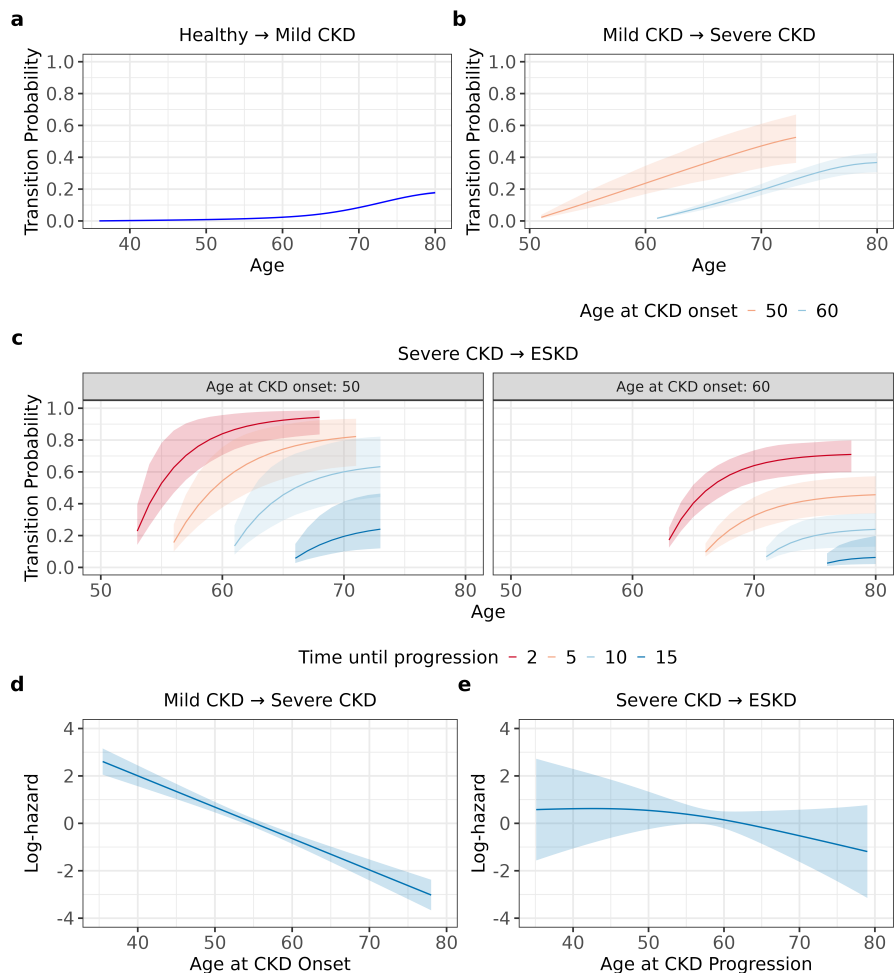


Figure 7: Transition probabilities and state-entry time effects for CKD onset and progression in UK Biobank. This figure shows transition probabilities (a-c) and the effects of state-entry times on transition log-hazards (d+e), estimated using an *SSTS* PAM on the UK Biobank data introduced in Section 5.1. Panel a shows "Healthy → Mild CKD" transition probabilities over age. Panel b shows "Mild CKD → Severe CKD" transition probabilities over age for different values of age at onset of Mild CKD (lines). Panel c shows "Severe CKD → ESKD" transition probabilities over age for different values of age at onset of Mild CKD (facets) and time until progression to Severe CKD (lines). Panels d and e show the zero-centered smooth effects of state-entry times (age at onset of Mild CKD and age at progression to Severe CKD) on the log-hazards of the respective transitions "Mild CKD → Severe CKD" and "Severe CKD → ESKD".

For transitions out of Severe CKD, we have additional dependence upon age_2 (age at progression to Severe CKD) and/or t_2 (time since onset of Mild CKD), with $age = age_2 + t_2$; see subject B of 2 with $age_2 = age_{progression}$ and $t_2 = time_{progression}$. Transition probabilities for "Severe CKD \rightarrow ESKD" rise with decreasing age_1 and age_2 ; that is, they are highest for subjects with early transitions into Mild and Severe CKD. Given age_1 and age_2 , the transition probabilities increase with age (Figures A.10 and A.11). "Severe CKD \rightarrow Death" transitions show a similar pattern as direct "Mild CKD \rightarrow Death" transitions (Figures A.12 and A.13).

We can now answer the first question from the very beginning: For a subject with onset of Mild CKD at age 50 and progression to Severe CKD at age 60, the probability of developing ESKD increases from 15% at age 61 to $> 60\%$ over the course of the next 10 years. Over the same period of time, the probability of dying rises from 5% to almost 30%.

Finally, we observe that the effects of state-entry times (here: age at CKD onset and progression) are mostly linear, though not always (Figures 7d+e and A.14). This underlines the importance of the modeling flexibility provided by this PAM-based framework.

5.3.2 Index event bias and genetic effect estimation

To investigate the effect of rs77924615 on CKD onset and progression, we use an *SSTS* PAM because we found this model robust to model misspecification (Section 4) and with better goodness of fit than the *MTS* PAM on this dataset (Section 5.3.1). In the naive model for testing this variant (omitting other risk factors), we observe a strong effect of rs77924615 on CKD onset log-hazards (+0.28), while its effect on log-hazards for progression to Severe CKD is seemingly protective (-0.12; Table 2).

However, these naive estimates are potentially subject to IEB due to the omission of other risk factors (cf. Section 4.2). For example, we observe a higher prevalence of diabetes and larger values of uACR for rs77924615 genotype AA compared to the other genotypes in state 2 (Table A.11).

The most straightforward approach is to directly adjust the model for other risk factors, under the assumption that all relevant other risk factors are known and observable and, thus, no unmeasured confounding remains after adjusting for them. Here we include sex, PGS, diabetes, smoking, BMI, and uACR (see Section 5.2). Inclusion of these risk factors leaves the genetic effect on CKD onset largely unchanged, while substantially attenuating the genetic effect on progression to Severe CKD from -0.12 to +0.05 (Table 2). Additionally, the stepwise inclusion of the above risk factors also improves the model fit in terms of the Akaike Information Criterion. So while there is sound evidence for a hazard-increasing effect of the *UMOD* genetic variant on CKD onset, there seems to be neither a detrimental nor a protective effect on CKD progression.

Table 2: Effect size estimates of the genetic variant rs77924615 on the log-hazards of CKD onset and progression in UK Biobank. This table shows effect sizes estimates along with standard errors and P-values for the genetic variant rs77924615 (effect allele G) on the log-hazards of the transitions 0→1 ("Healthy → Mild CKD"), 1→2 ("Mild CKD → Severe CKD"), and 2→3 ("Severe CKD → ESKD"), in the UK Biobank dataset introduced in Section 5.1. The models are estimated using an *SSTS* PAM as specified in Section 5.2, with additional risk factors as stated in the column Risk Factors. Quantitative risk factors (PGS, BMI, uACR) are modeled via penalized splines ($k = 20$).

Risk Factors	Transition	Coefficient	SE	P-value
G only (AIC: 202,984)	0→1	0.284	0.025	<0.001
	1→2	-0.121	0.090	0.181
	2→3	-0.311	0.146	0.034
G + Sex (AIC: 202,275)	0→1	0.284	0.025	<0.001
	1→2	-0.111	0.091	0.222
	2→3	-0.330	0.146	0.024
G + Sex + PGS (AIC: 201,845)	0→1	0.282	0.025	<0.001
	1→2	-0.113	0.091	0.214
	2→3	-0.330	0.146	0.024
G + Sex + PGS + Diabetes (AIC: 201,644)	0→1	0.283	0.025	<0.001
	1→2	-0.107	0.091	0.237
	2→3	-0.331	0.146	0.024
G + Sex + PGS + Diabetes + Smoking (AIC: 184,976)	0→1	0.280	0.026	<0.001
	1→2	-0.086	0.095	0.364
	2→3	-0.243	0.175	0.166
G + Sex + PGS + Diabetes + Smoking + BMI AIC: (182,436)	0→1	0.288	0.026	<0.001
	1→2	-0.111	0.095	0.243
	2→3	-0.230	0.174	0.187
G + Sex + PGS + Diabetes + Smoking + BMI + uACR (AIC: 175,181)	0→1	0.278	0.026	<0.001
	1→2	0.045	0.100	0.654
	2→3	-0.159	0.178	0.371

G: Genetic variant rs77924615 (effect allele G).
0: Healthy; 1: Mild CKD; 2: Severe CKD; 3: ESKD.
AIC: Akaike Information Criterion.

This answers the second question posed at the very beginning of this paper.

An alternative to the direct adjustment for other risk factors is to use propensity scores to compute subject- and state-specific stabilizing weights for the estimation of a weighted PAM (Appendix A.2.1). This weighting approach produces similar results as the adjustment approach regarding the estimation of rs77924615 effects on CKD onset and progression (Table A.12). However, we note that the incorporation of time-varying covariates requires the estimation

of time-varying weights and, while feasible, is much more complex [63, 64, 65].

5.3.3 Evaluating the impact of interval-censoring on the CKD multi-state model estimation

Due to the dense eHRs in our dataset (median time between eGFR measurements: 1.44 years), the overall degree of interval-censoring is limited. Furthermore, death time points are not affected by interval-censoring as the corresponding information stems from exactly recorded death registries. As expected, we observe informative observation [43, 44] as interval length is related to CKD stage (median time between observations: 1.46, 0.68, and 0.27 years for Healthy, Mild CKD, and Severe CKD, respectively). This means that less healthy individuals – i.e., those who are more likely to have CKD-related events – tend to have more detailed eHR trajectories and, hence, smaller interval lengths (cf. Section 2.4). As suggested in the literature [cf. 9, Section 5.4], Poisson processes can be used to handle informative observation – and our PAM-based framework is inherently linked to a Poisson process via likelihood equivalence. In addition, the flexibility of our non-Markov framework allows for further mitigation of any potential biases from informative observation via direct incorporation of (history-dependent, time-varying) characteristics of the observation process into the model – for example in the form of the number of visits or mean inter-visit time.

We perform sensitivity analyses on the results in Section 5.3.2 by using two different estimation points – interval mid- versus end-points – as event times and evaluating the impact on risk factor effect size estimates. As can be seen in Table A.13, estimates are similar for mid- and end-point estimation – as expected based on the results from Section 4.3.2.

6 Discussion

In this work, we investigated the analysis of multi-stage disease histories via multi-state models, along with the resulting statistical challenges and their impact on model estimation. Via simulation studies and a real-world application in UKB, we demonstrated that most of these challenges can be addressed within a PAM-based modeling framework. This framework facilitates: adjustment for dependent left-truncation by including state-entry times; accommodation of multiple time scales while ensuring identifiability; seamless incorporation of time-varying covariates (and effects) to account for OVB and IEB; and flexible non-linear effect estimation.

Regarding the choice of time scales, a stratified single time scale proved more robust to model misspecification in terms of baseline hazard estimation than using multiple time scales. The *SSTS* PAM also showed a better fit on the empirical data from UKB. Interestingly, this is also in line with the leukemia example by Iacobelli and Carstensen [22], whose final model eventually does not

contain multiple time scales either. Therefore, a relatively simple (single time scale) model appears to suffice even for estimation of hazards from complex DGPs with multiple time scales. In terms of estimating the hazards of fixed effects (e.g., risk factors), both approaches were found to be robust.

As all non-initial states in a multi-state model are restricted to index events, IEB is of particular importance. We demonstrated the induction of negative correlation within a "diseased subpopulation" between risk factors that are independent in the healthy population. This caused attenuation bias when one of the risk factors was omitted from the model. We then showed that this bias can be corrected for by including the omitted risk factor into the model or by using a propensity score-based weighting approach. The PAM framework facilitates flexible covariate adjustment as well as weighting.

Furthermore, we showed that PAMs – using interval mid-points as estimation points – recovered fixed effect hazards very well even with interval-censored data, making this framework particularly suitable to disease histories derived from longitudinal data.

On UKB data, *SSTS* and *MTS* PAMs mostly produced similar estimates of CKD onset and progression hazards and transition probabilities. In particular, we found progression risk to Severe CKD to be highest for subjects with early onset of Mild CKD and to further rise with age. From there, the risk of further progressing to ESKD was highest for subjects with early onset of Mild CKD and progression to Severe CKD, again increasing with age. We also found the *G* allele of the genetic variant rs77924615 (*UMOD* locus) to increase the risk of CKD onset, in line with literature [66, 31]. Importantly, we observed an initial protective effect of this *G* allele on progression into Severe CKD and ESKD; yet this effect disappeared after adjustment for other risk factors of CKD and CKD progression. The initial protective effect thus seems to be attributable to IEB.

However, we also identified limitations, which in turn provide opportunities for future research.

First, the individual simulation setups could be expanded even further. The simulations regarding choice of time scales and IEB, for instance, could be enhanced by also considering other DGPs beyond the piecewise exponential distribution – though we do note that the latter one is particularly flexible and that the simulations on interval-censoring underlined the ability of PAMs to adequately estimate multiple distinct baseline hazards. In addition, it would be interesting to expand the IEB simulations to scenarios with dependence structures between risk factors in the healthy population. In particular, for specific application settings it could be informative to directly use empirical joint distributions of risk factors for simulations.

Second, the recovery of baseline hazards by PAMs under interval-censoring is still suboptimal. This is because direct incorporation of interval-censoring into the PEM likelihood, while maintaining its proportionality to a Poisson likelihood, remains a challenge. In this context, it would also be of interest to conduct further simulations regarding the impact of interval-censoring within

complex multi-state model settings, because interval-censored transition times out of the initial state also induce censoring in the observed state-entry times of subsequent states.

Third, our proposed handling of IEB relies upon other risk factors being observable and on the assumption of no unmeasured confounding to remain after risk factor adjustment. Both of these are often not (or only partially) the case: In our UKB dataset, for instance, the risk factors BMI and uACR are available only from study center assessments, but not from eHRs; and in addition, it is very likely that further (unknown, unaccounted for) risk factors exist, which is why some degree of unmeasured confounding cannot be ruled out here. And while off-the-shelf bias correction methods for linear and binary outcomes exist [67, 68, 69], their applicability to multi-state models is still to be explored.

Finally, as UKB participants are rather healthy [70], CKD progressions in this UKB dataset are relatively rare. This, in turn, makes the estimation of (especially small-scale, genetic) risk factors more difficult. It would thus be interesting to conduct similar CKD onset and progression analyses in less healthy cohorts.

Data availability

The UK Biobank analyses in Section 5 were conducted under the application numbers 20272 and 23940. UK Biobank is a publicly accessible database. Individual participant data from UKB is available via the UK Biobank resource.

Code availability

Multi-state PAMs (including all necessary preprocessing) are implemented in the R package `pamtools` [25], which uses `mgcv::gam()/bam()` [53] for efficient and flexible estimation. All code required for running the simulations (Section 4), for the UK Biobank analyses (Section 5), as well as for creating the corresponding figures and tables, is available from the GitHub repository <https://github.com/survival-org/msm4diseaseHistories>.

A Appendix

A.1 Additional information on the flexible modeling of disease histories using piecewise exponential additive models

A.1.1 Transformation to piecewise exponential data

The preprocessing step to transform standard survival data into the PED format starts by partitioning the follow-up time into J intervals $(0 = a_0, a_1], (a_1, a_2], \dots, (a_{j-1}, a_j], \dots, (a_{J-1}, a_J]$ using cut points $a_0 < a_1 < \dots < a_{J-1} < a_J$. $I_j := (a_{j-1}, a_j]$ denotes the j -th time interval and $J_i \in \{1, \dots, J\}$ indexes the time interval for which y_i was observed ($y_i \in I_{J_i} = (a_{J_i-1}, a_{J_i}]$). Using this partitioning, the original dataset is transformed into the long-form PED, which contains one row for each unique combination of subject i and interval-at-risk j ($\forall j \in \{1, \dots, J_i\}$), as well as the following newly introduced variables:

- an event indicator $d_{ij} = \begin{cases} 1 & \text{if } y_i \in I_j \wedge d_i = 1 \\ 0 & \text{else} \end{cases}$,
- the time at risk $y_{ij} = \begin{cases} a_j - a_{j-1} & \text{if } a_j < y_i \\ y_i - a_{j-1} & \text{if } a_{j-1} < y_i \leq a_j \end{cases}$,
- and an "offset" $o_{ij} = \log(y_{ij})$.

Note that accounting for left-truncation, time-varying covariates, and time-varying effects all require similar data transformations and can therefore seamlessly be incorporated into this data preprocessing step [27]. To capture changes in time-varying covariates accurately, additional time cut points can be added at times where the time-varying covariates change [25].

PEMs then use $d_{ij} \sim Po(\mu_{ij})$ as outcome of a Poisson regression model with expected conditional event rate $\mu_{ij} = h_{ij}y_{ij}$ and logarithmized time-at-risk entering as offset o_{ij} , to estimate the hazard rate h_{ij} as the product of a piecewise constant baseline hazard rate (for each interval) and the exponential of a linear predictor. PEMs can be shown to be equivalent to the Cox Proportional Hazards model under certain assumptions [71], but since they do not rely on the non-parametric estimation of the baseline hazard (due to assuming piecewise-constant hazards), they are fully parametric with respect to parameter estimation. Still, we here refer to PEMs as semi-parametric approach, analogously to the Cox model, because no parametric event time distribution is assumed - in contrast to parametric approaches such as Accelerated Failure Time models [72].

A.1.2 Augmentation of piecewise exponential data for multi-state models

To simplify the multi-state process, we begin by analyzing each state separately, thereby reducing the problem to a set of nested competing risks models. Specif-

ically, for each state ℓ , we assume there are q_ℓ possible transitions - each corresponding to a competing risk. For each of these q_ℓ competing risks (transitions), we construct a separate dataset. In the dataset corresponding to transition k , we replace the event indicator d_{ij} by a cause-specific event indicator:

$$d_{ijk} = \begin{cases} 1 & \text{if } d_{ij} = 1 \text{ and } d_{ik} = 1, \\ 0 & \text{otherwise} \end{cases}$$

where d_{ik} is a binary indicator of whether the event was of type k . Effectively, in the k -th dataset all other transitions $\tilde{k} \neq k$ are thus treated as censored. This data transformation step can also be interpreted as an augmentation procedure involving counterfactual transitions, where, for each possible transition k , we consider what would happen under the assumption that only k were observable. As subjects enter transition-specific risk sets at different points in time, the multi-state transformation accounts for this left-truncation by including the state entry time in addition to the transition time y_{ij} . In case of multiple visits to a state (due to recurrent events), episode e can be added to the transformed data as additional column. Finally, all state-specific datasets are stacked.

A.2 Additional information on CKD onset and progression analyses in UK Biobank

A.2.1 Propensity score-based correction for index event bias

The idea of the weighting approach is to create subject- and state-specific (i.e., transition-specific) weights that reflect how likely a subject is to have a certain rs77924615 genotype, given the values of their other risk factors. These weights can then be fed as an argument into the PAM estimation algorithm.

To calculate the weights, we first compute the marginal probability of a subject having their true rs77924615 genotype (versus not having it), separately for each from-state. This is identical to the state-specific relative frequency of that genotype. Second, we compute the propensity score - the probability of a subject having their true rs77924615 genotype (versus not having it), given their set of risk factors and the from-state - via multinomial logistic regression. The weights are calculated by dividing the subject- and state-specific relative frequency of the genotype by the respective propensity score. A large weight means that a subject, given their risk factors and the from-state, is unlikely to have a certain genotype; such an observation is accordingly up-weighted during model estimation.

A.3 Supplementary figures

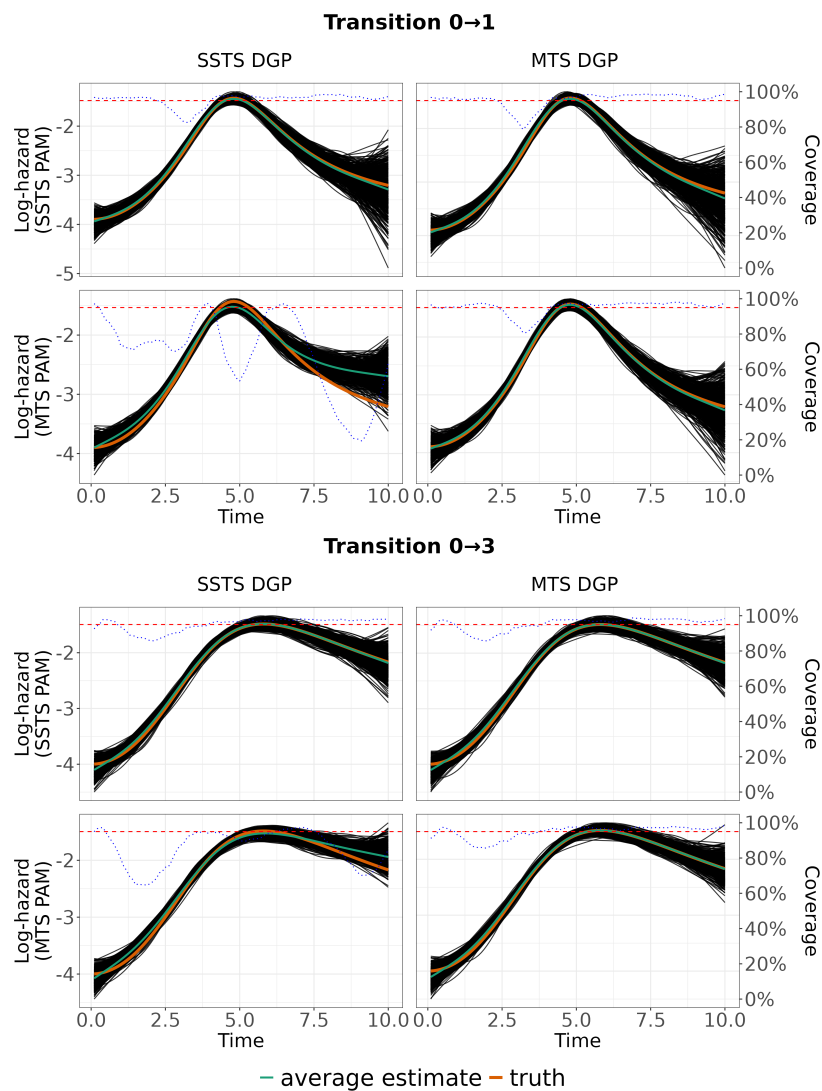


Figure A.1: Line plots and coverage of *SSTS* and *MTS* PAMs on data simulated from *SSTS* and *MTS* DGPs. This figure shows line plots (solid black lines) and point-wise coverage (dotted blue line) of baseline log-hazards for the transitions $0 \rightarrow 1$ (top) and $0 \rightarrow 3$ (bottom), estimated on data simulated from an *SSTS* DGP (left) and an *MTS* DGP (right), using either an *SSTS* PAM or an *MTS* PAM (only penalized splines smooth for illustration). The green and orange lines represent average estimates and the true log-hazard, respectively. The dashed red line corresponds to nominal (95%) coverage.

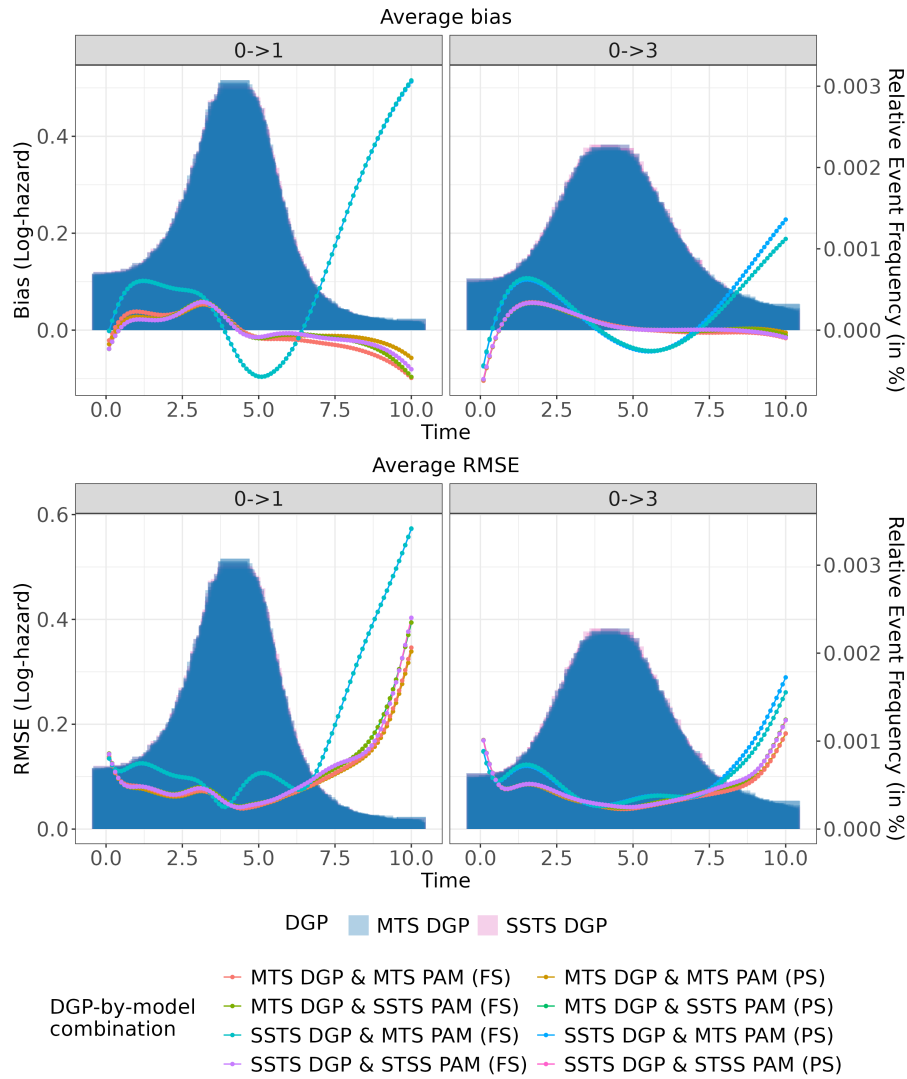


Figure A.2: Bias and RMSE of *SSTS* and *MTS* PAM-based log-hazards over time on data simulated from *SSTS* and *MTS* DGPs. This figure shows log-hazard bias and RMSE (left y-axis) over time (x-axis) and averaged across simulation runs for the transitions $0 \rightarrow 1$ (top) and $0 \rightarrow 3$ (bottom), estimated on data simulated from an *SSTS* DGP and an *MTS* DGP, using either an *SSTS* PAM or an *MTS* PAM and either a penalized splines smooth or a factor smooth. In addition, this figure shows relative event frequencies over time (averaged across simulation runs; right y-axis) for these two transitions and each of the two DGPs.

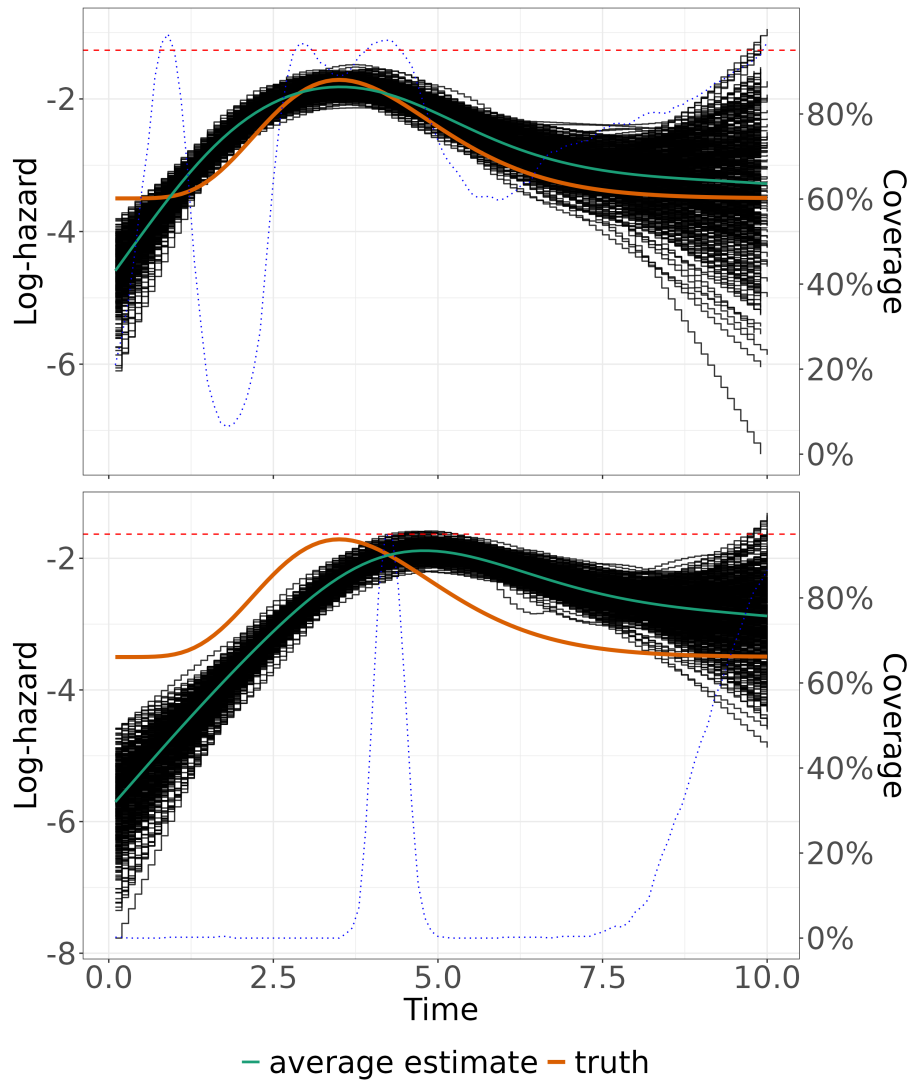


Figure A.3: Line plots and point-wise coverage of PAM-based log-hazards over time under interval-censoring using interval mid- and end-points. This figure shows line plots (in black) of log-hazards on data simulated from a piecewise exponential DGP with beta IC mechanism, estimated using PAMs with interval mid-points (top) and end-points (bottom) as estimation points. The green and orange lines represent average estimates and the true log-hazard, respectively. The dotted blue line denotes pointwise coverage. The dashed red line corresponds to nominal (95%) coverage.

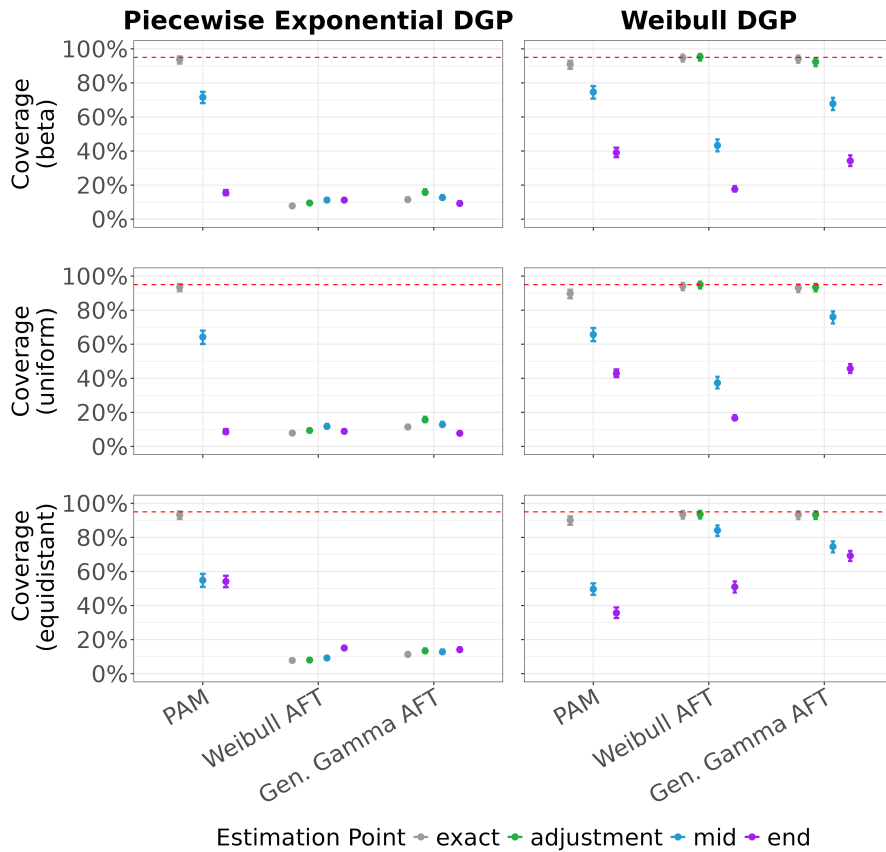


Figure A.4: Mean coverage of baseline log-hazards under interval-censoring. This figure shows mean baseline log-hazard coverage of three models (x-axis) using three to four distinct estimation points (color coding) on data generated by two DGPs (columns) and three IC mechanisms (rows), based on the simulation setup described in Section 4.3.1. For each model and combination of DGP and IC mechanism, the dot and error bars represent mean coverage and 95% confidence intervals (from an exact binomial test), computed pointwise across all simulation runs and then averaged over time points. The dashed red line corresponds to nominal (95%) coverage. The results from the `icenReg`-based DGP are similar to those from the Weibull-based DGP with uniform IC mechanism (see Table A.6).

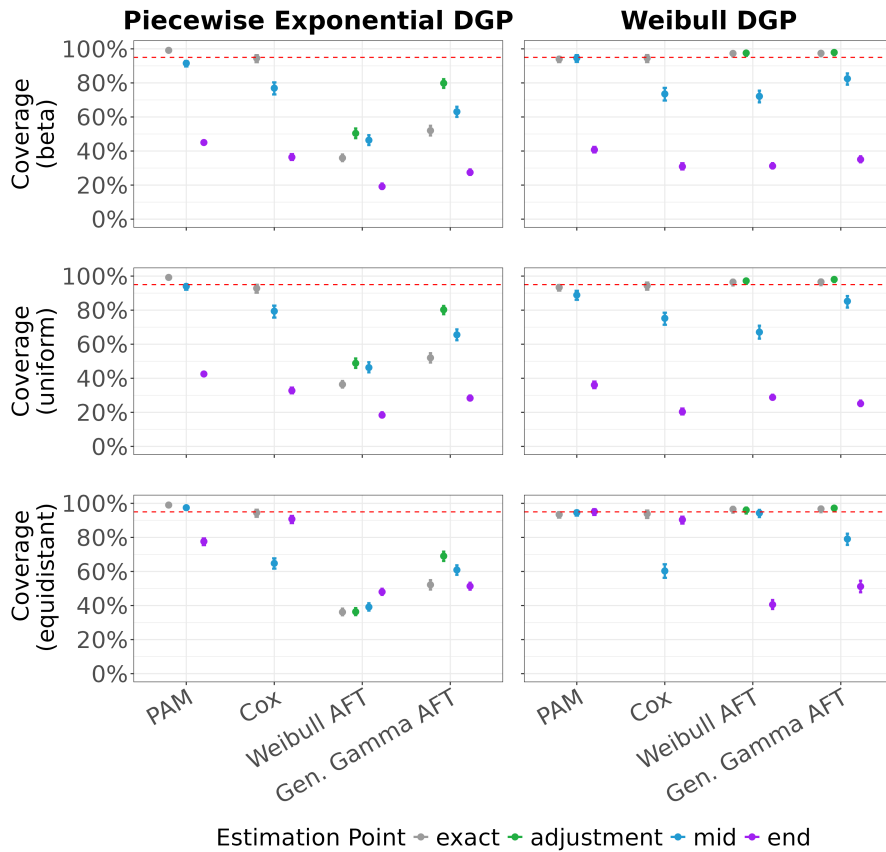


Figure A.5: Mean coverage of baseline cumulative hazards under interval-censoring. This figure shows mean baseline cumulative hazard coverage of four models (x-axis) using three to four distinct estimation points (color coding) on data generated by two DGPs (columns) and three IC mechanisms (rows), based on the simulation setup described in Section 4.3.1. For each model and combination of DGP and IC mechanism, the dot and error bars represent mean coverage and 95% confidence intervals (from an exact binomial test), computed pointwise across all simulation runs and then averaged over time points. The dashed red line corresponds to nominal (95%) coverage. The results from the `icenReg`-based DGP are similar to those from the Weibull-based DGP with uniform IC mechanism (see Table A.6).

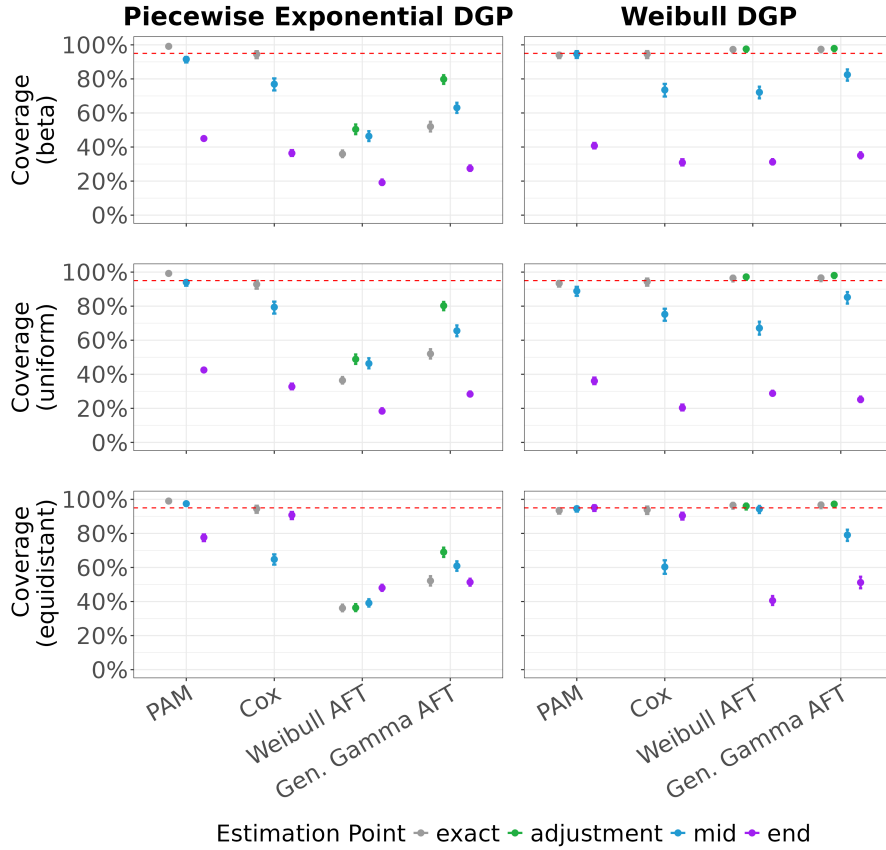


Figure A.6: Mean coverage of baseline survival functions under interval-censoring. This figure shows mean baseline survival function coverage of four models (x-axis) using three to four distinct estimation points (color coding) on data generated by two DGPs (columns) and three IC mechanisms (rows), based on the simulation setup described in Section 4.3.1. For each model and combination of DGP and IC mechanism, the dot and error bars represent mean coverage and 95% confidence intervals (from an exact binomial test), computed pointwise across all simulation runs and then averaged over time points. The dashed red line corresponds to nominal (95%) coverage. The results from the `icenReg`-based DGP are similar to those from the Weibull-based DGP with uniform IC mechanism (see Table A.6).

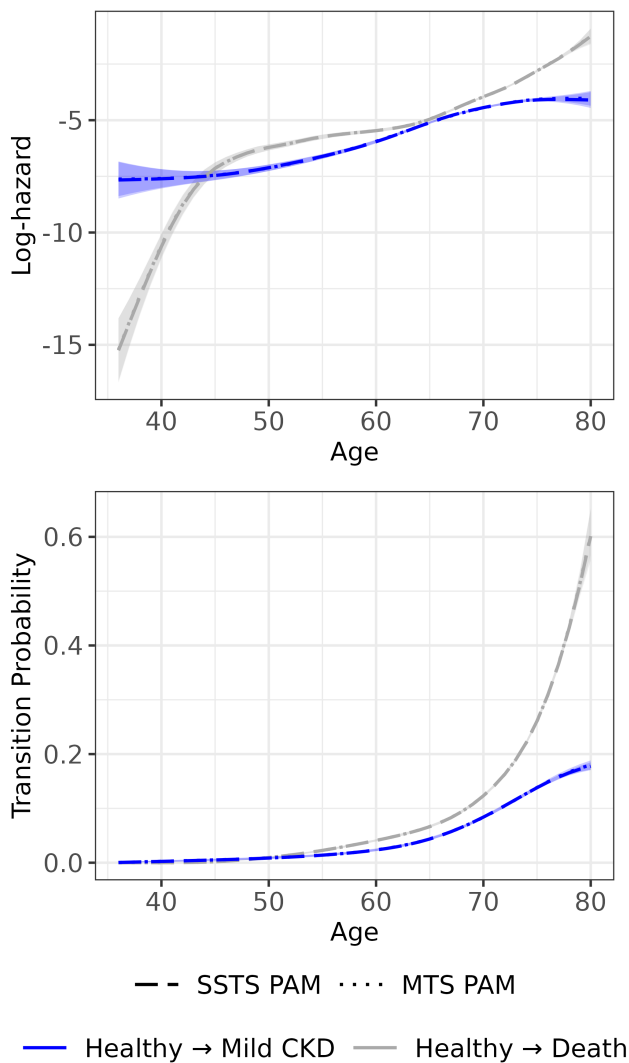


Figure A.7: Predicted log-hazards and transition probabilities over age for transitions "Healthy → Mild CKD" and "Healthy → Death" in UK Biobank. This figure shows log-hazards (top) and transition probabilities (bottom) for the transitions from state Healthy into states Mild CKD (grey lines) and Death (blue lines), estimated using an *SSTS* PAM (dashed lines) and an *MTS* PAM (dotted lines) on the UK Biobank data introduced in Section 5.1. Shades depict 95% confidence bands.

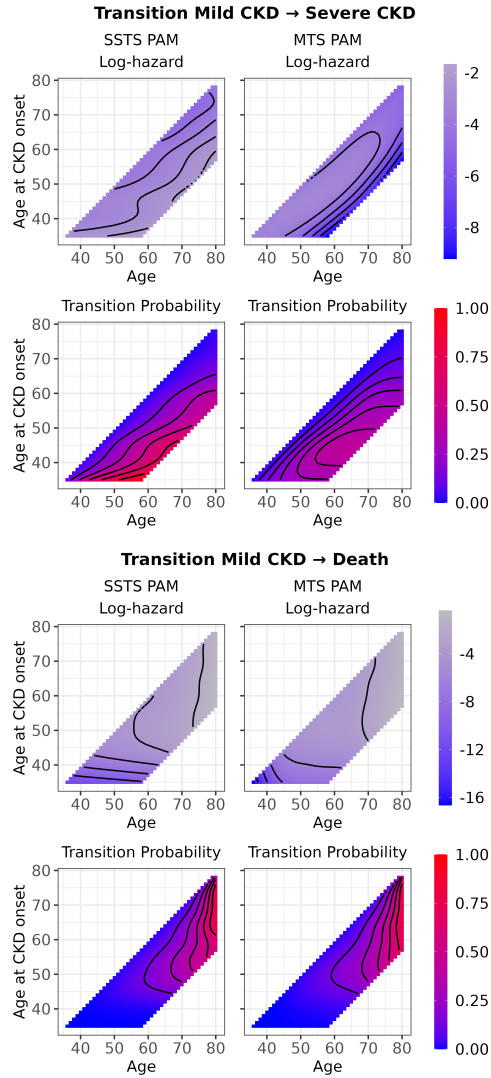


Figure A.8: Contour plots of predicted log-hazards and transition probabilities over age and age at CKD onset for transitions "Mild CKD \rightarrow Severe CKD" and CKD \rightarrow Death in UK Biobank. For the direct transitions from Mild CKD to Severe CKD (top) and Death (bottom), this figure shows contour plots of log-hazards (top rows) and transition probabilities (bottom rows) over age and age at CKD onset, estimated using an *SSTS* PAM (left column) and an *MTS* PAM (right column) on the UK Biobank data introduced in Section 5.1. By definition, age must exceed age at CKD onset. Prediction horizons within Mild CKD are restricted to the empirically observed range (time since CKD onset $\in [0, 23]$ years). Grey lines represent contour lines.

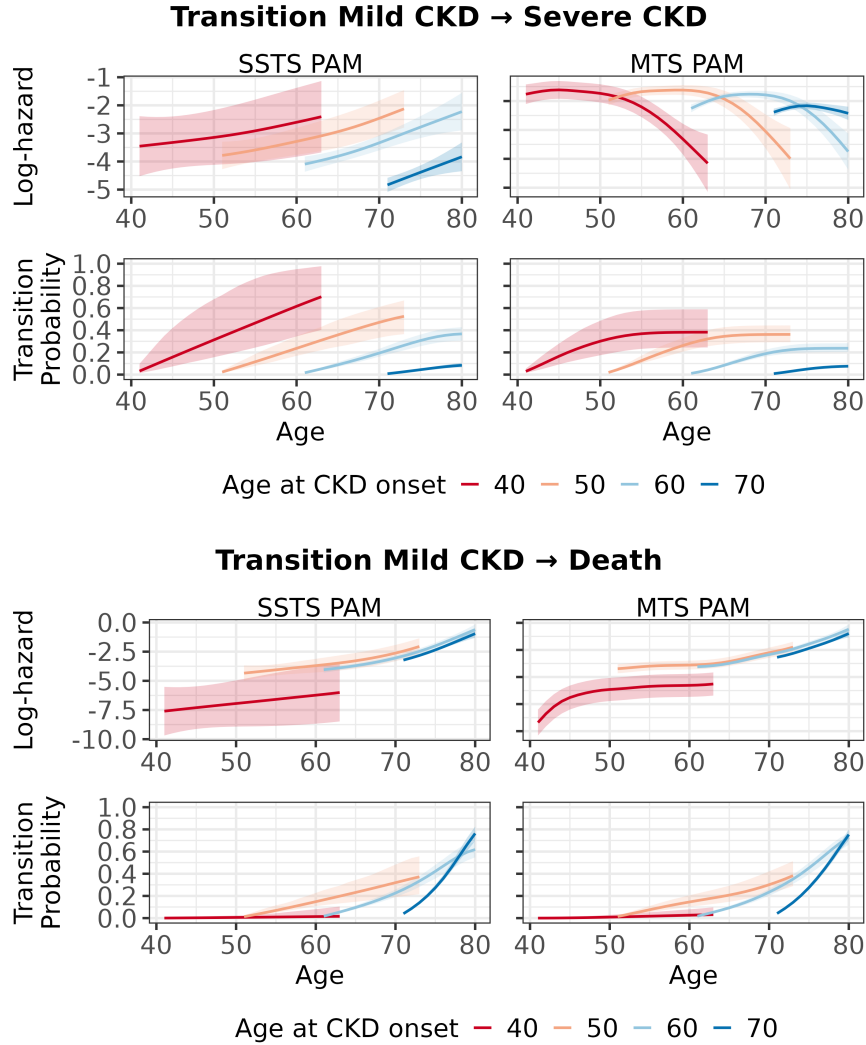


Figure A.9: Slice plots of predicted log-hazards and transition probabilities for transitions "Mild CKD → Severe CKD" and CKD → Death over age for different values of age at CKD onset in UK Biobank. For the direct transitions from Mild CKD to Severe CKD (top) and Death (bottom), this figure shows slice plots of log-hazards (top rows) and transition probabilities (bottom rows) over age for four distinct values of age at CKD onset, estimated using an *SSTS* PAM (left column) and an *MTS* PAM (right column) on the UK Biobank data introduced in Section 5.1. Shades depict 95% confidence bands. By definition, age must exceed age at CKD onset. Prediction horizons within Mild CKD are restricted to the empirically observed range (time since CKD onset $\in [0, 23]$ years).

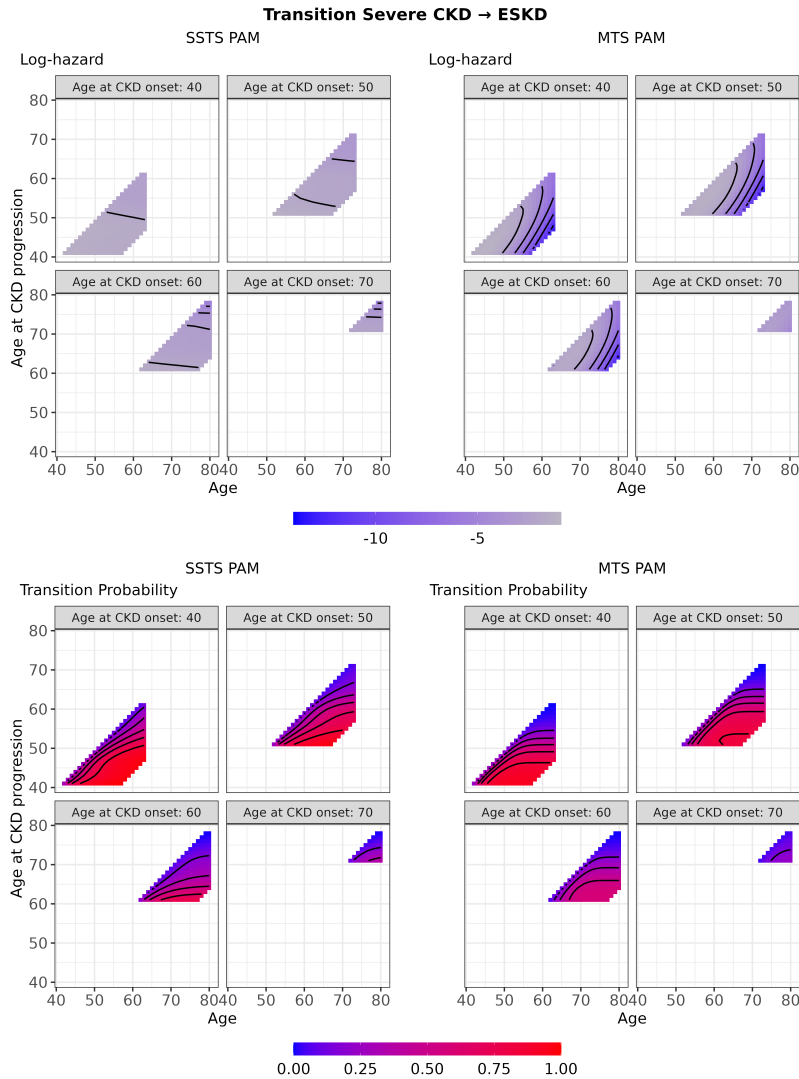


Figure A.10: Contour plots of predicted log-hazards and transition probabilities for transition "Severe CKD → ESKD" over age and age at CKD progression for different values of age at CKD onset in UK Biobank. For the transition "Severe CKD → ESKD", this figure shows contour plots of log-hazards (top) and transition probabilities (bottom) over age and age at progression to Severe CKD for four distinct values of age at CKD onset, estimated using an *SSTS* PAM (left column) and an *MTS* PAM (right column) on the UK Biobank data introduced in Section 5.1. By definition, age must exceed age at CKD onset and progression and age at CKD progression must exceed age at CKD onset. Prediction horizons within Severe CKD are restricted to the empirically observed range (time since CKD progression $\in [0, 16]$ years). Grey lines represent contour lines.

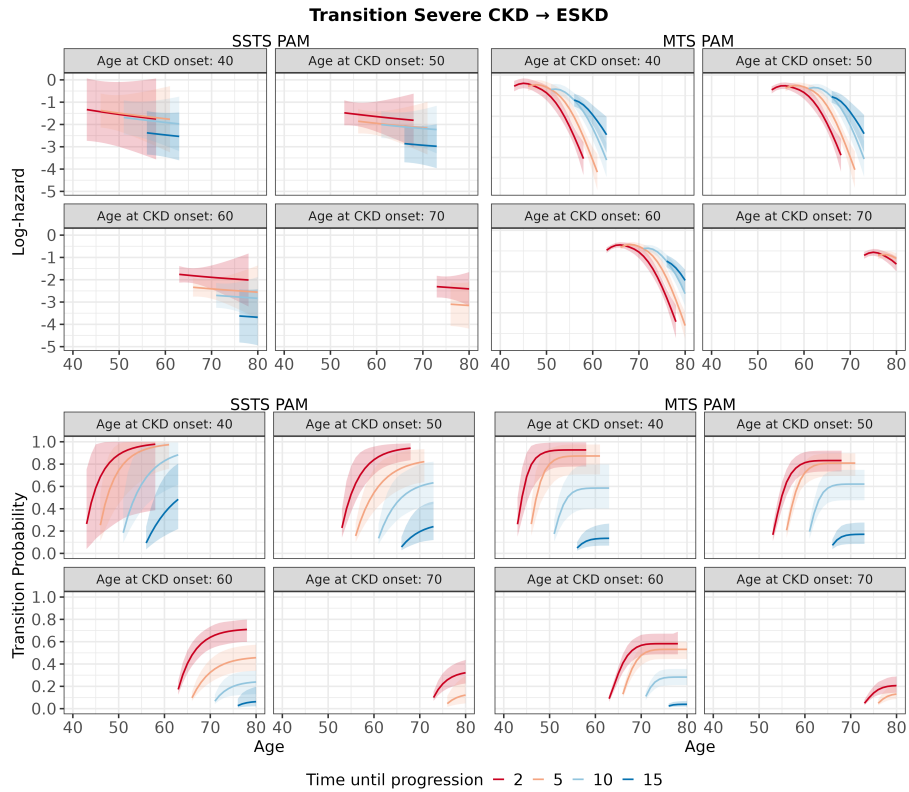


Figure A.11: Slice plots of predicted log-hazards and transition probabilities for transition "Severe CKD → ESKD" over age for different values of age at CKD onset and time until CKD progression in UK Biobank. For the transition "Severe CKD → ESKD", this figure shows slice plots of log-hazards (top) and transition probabilities (bottom) over age, for four distinct values of age at CKD onset (facets) and time until CKD progression (colors), estimated using an *SSTS* PAM (left column) and an *MTS* PAM (right column) on the UK Biobank data introduced in Section 5.1. Shades depict 95% confidence bands. By definition, age must exceed age at CKD onset and progression and age at CKD progression must exceed age at CKD onset. Prediction horizons within Severe CKD are restricted to the empirically observed range (time since CKD progression $\in [0, 16]$ years).

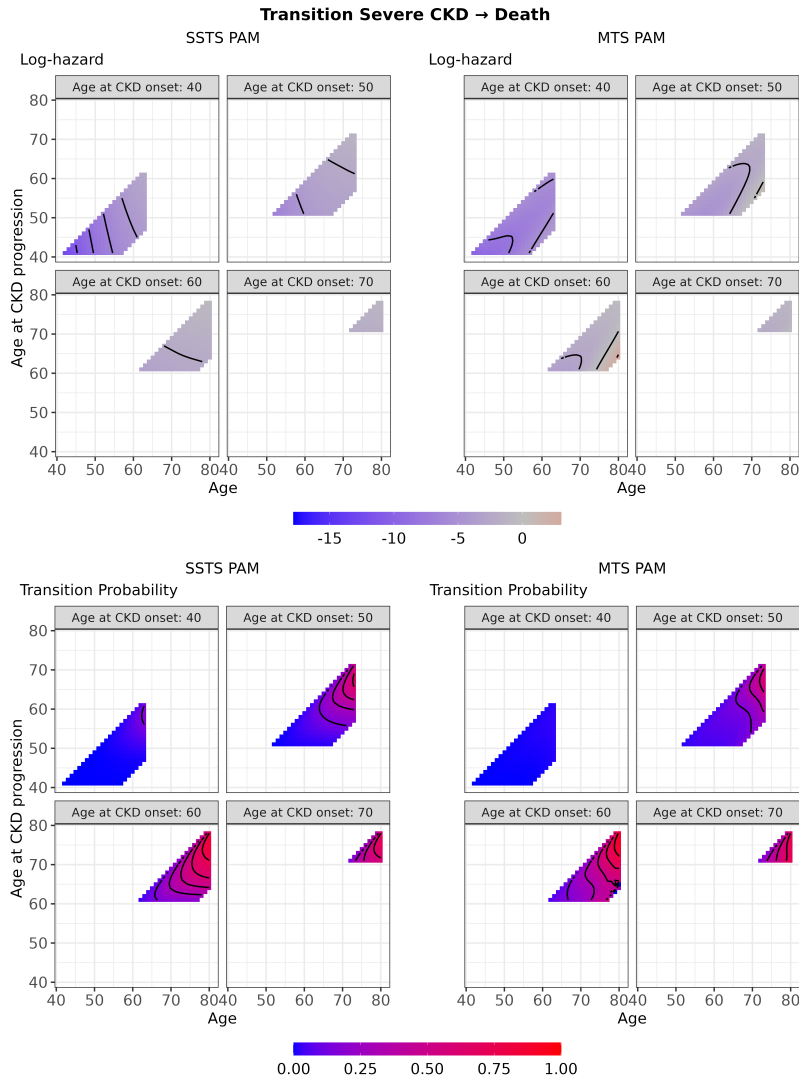


Figure A.12: Contour plots of predicted log-hazards and transition probabilities for transition "Severe CKD → Death" over age and age at CKD progression for different values of age at CKD onset in UK Biobank. For the transition "Severe CKD → Death", this figure shows contour plots of log-hazards (top) and transition probabilities (bottom) over age and age at progression to Severe CKD for four distinct values of age at CKD onset, estimated using an *SSTS* PAM (left column) and an *MTS* PAM (right column) on the UK Biobank data introduced in Section 5.1. By definition, age must exceed age at CKD onset and progression and age at CKD progression must exceed age at CKD onset. Prediction horizons within Severe CKD are restricted to the empirically observed range (time since CKD progression $\in [0, 16]$ years). Grey lines represent contour lines.

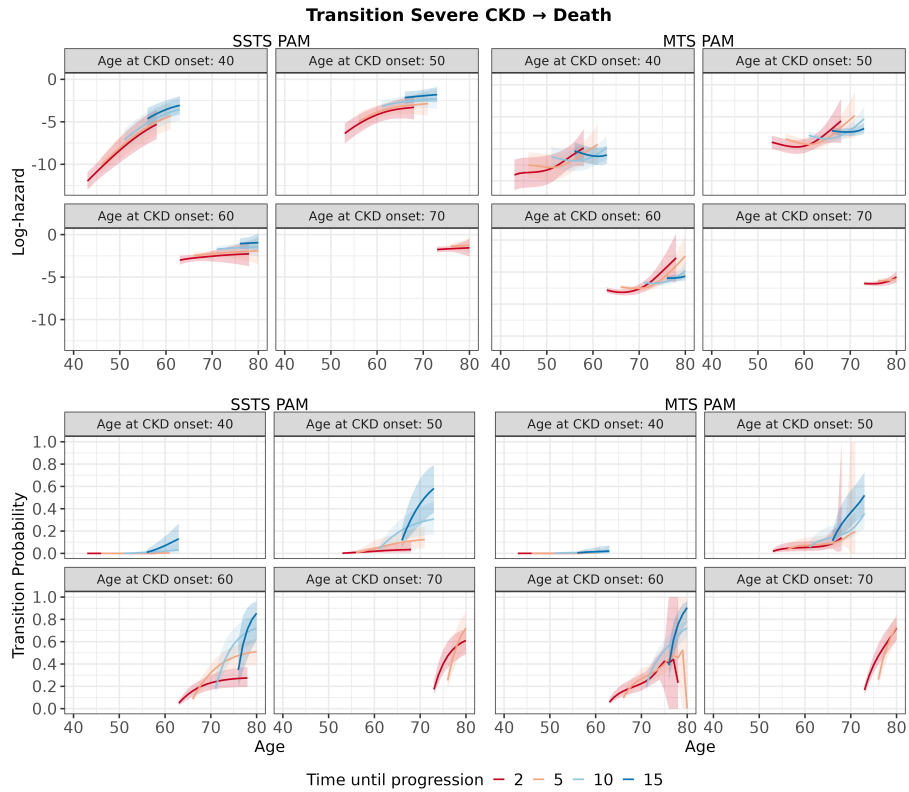


Figure A.13: Slice plots of predicted log-hazards and transition probabilities for transition "Severe CKD → Death" over age for different values of age at CKD onset and time until CKD progression in UK Biobank. For the transition "Severe CKD → Death", this figure shows contour plots of log-hazards (top) and transition probabilities (bottom) over age, for four distinct values of age at CKD onset (facets) and time until CKD progression (colors), estimated using an *SSTS* PAM (left column) and an *MTS* PAM (right column) on the UK Biobank data introduced in Section 5.1. Shades depict 95% confidence bands. By definition, age must exceed age at CKD onset and progression and age at CKD progression must exceed age at CKD onset. Prediction horizons within Severe CKD are restricted to the empirically observed range (time since CKD progression $\in [0, 16]$ years).

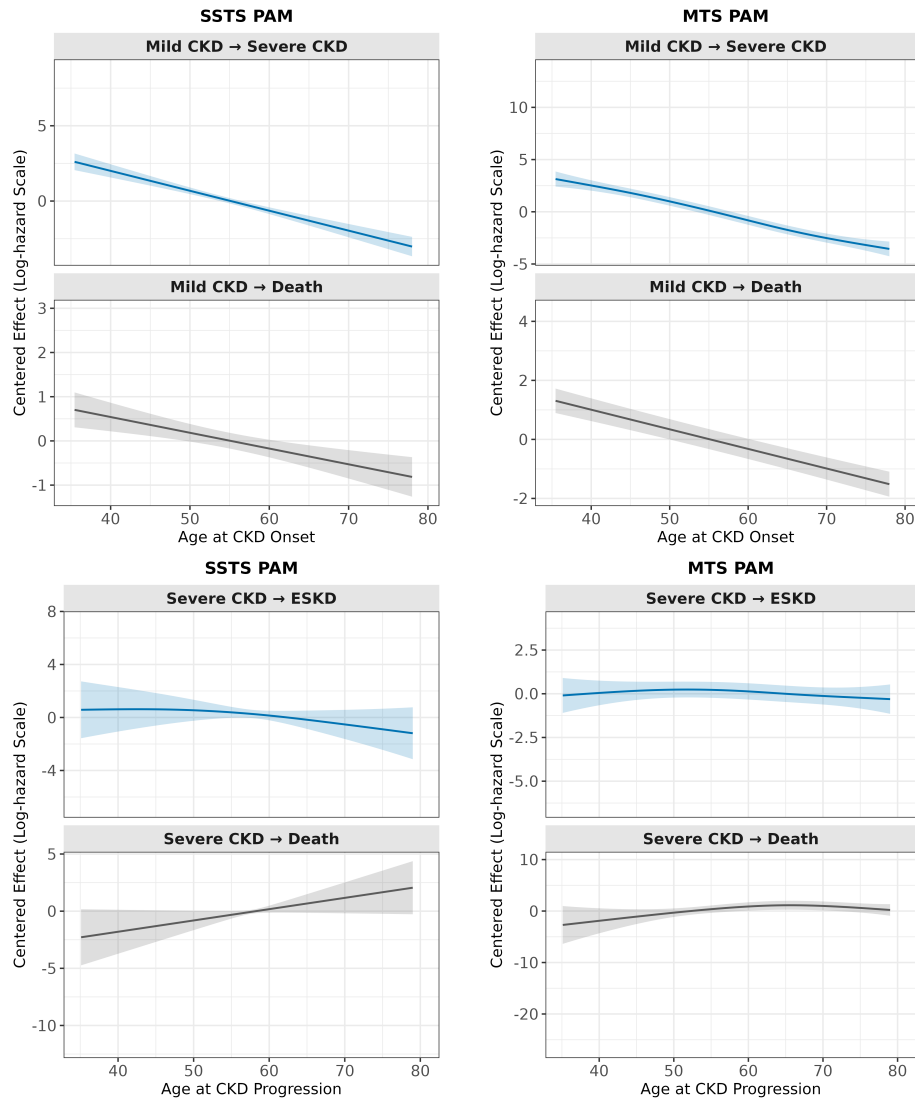


Figure A.14: Centered effects of state-entry times on transitions out of states Mild and Severe CKD in UK Biobank. This figure shows centered effect plots for the effect of state-entry times on log-hazards, estimated with an *SSTS* PAM (left) or an *MTS* PAM, on UK Biobank data. The two top rows correspond to effects of left-truncation variable age at CKD onset on the log-hazards of transitions out of state Mild CKD (to Severe CKD or Death). The two bottom rows correspond to effects of left-truncation variable age at CKD progression on the log-hazards of transitions out of state Severe CKD (to ESKD or Death).

A.4 Supplementary tables

Table A.1: Details on data generating processes. This table provides detailed information on the baseline hazard functions and fixed effect parameters of the data generating processes employed in Section 4.1 (see Equations (8), (9) and (10)). The *SSTS* DGP has one time-varying baseline log-hazard $f_k^{ssts}(t)$ per transition $k \in \{0 \rightarrow 1, 0 \rightarrow 3, 1 \rightarrow 2, 1 \rightarrow 3\}$, i.e., a total of four. For the *MTS* DGP, we also have four time scale functions: Functions $f_0^{mts}(t)$ and $f_1^{mts}(t_1)$ represent the time-varying baseline log-hazard of time since study entry on transition $0 \rightarrow 1$ (*onset*; first time scale) and of time since onset on transition $1 \rightarrow 2$ (*progression*; second time scale). Functions $\tilde{f}_0^{mts}(t)$ and $\tilde{f}_1^{mts}(t_1)$ represent the time-varying baseline log-hazard of time since study entry on transition $0 \rightarrow 3$ (first time scale) and of time since onset on $1 \rightarrow 3$ (second time scale). For transitions out of state 1, the components $f_0^{mts}(t)$ and $f_1^{mts}(t_1)/\tilde{f}_1^{mts}(t_1)$ are then added up. $f_{\text{until}_1}(t_{\text{until}_1})$ and $\tilde{f}_{\text{until}_1}(t_{\text{until}_1})$ are shared across the two DGPs and represent the effect of the time until onset t_{until_1} on transitions $1 \rightarrow 2$ and $1 \rightarrow 3$, respectively. The fixed effect parameters $\beta_{0,k}$ and $\beta_{x_1,k}$ are transition-specific intercepts and covariate fixed effects on the log-hazard level, shared across the two DGPs.

Parameter	Definition
<i>Time-Dependent Baseline Hazard Functions</i>	
$f_{0 \rightarrow 1}^{ssts}(t)$	$= \frac{0.10t^2}{0.7+0.04(\max\{0,t-3\})^3}$
$f_{0 \rightarrow 3}^{ssts}(t)$	$= \frac{0.15t^2}{0.9+0.01(\max\{0,t-1\})^3}$
$f_{1 \rightarrow 2}^{ssts}(t)$	$= 0.48e^{-0.10t}$
$f_{1 \rightarrow 3}^{ssts}(t)$	$= 0.16e^{-0.30t}$
$f_{02}^{mts}(t)$	$= f_{0 \rightarrow 1}^{ssts}(t)$
$f_{12}^{mts}(t_1)$	$= 0.32e^{-0.15t_1}$
$\tilde{f}_{03}^{mts}(t)$	$= \tilde{f}_{0 \rightarrow 3}^{ssts}(t)$
$\tilde{f}_{13}^{mts}(t_1)$	$= 0.14e^{-0.25t_1}$
$f_{\text{entry}_1}(t_{\text{entry}_1})$	$= 2.50e^{-0.60t_{\text{entry}_1}}$
$\tilde{f}_{\text{entry}_1}(t_{\text{entry}_1})$	$= 0.14e^{-0.25t_{\text{entry}_1}}$
<i>Fixed Effect Parameters</i>	
$\beta_{0,0 \rightarrow 1}$	$= -3.9$
$\beta_{0,0 \rightarrow 3}$	$= -4.0$
$\beta_{0,1 \rightarrow 2}$	$= -3.4$
$\beta_{0,1 \rightarrow 3}$	$= -3.4$
$\beta_{x_1,0 \rightarrow 1}$	$= 0.2$
$\beta_{x_1,0 \rightarrow 3}$	$= 0.1$
$\beta_{x_1,1 \rightarrow 2}$	$= 0.2$
$\beta_{x_1,1 \rightarrow 3}$	$= 0.1$

Table A.2: Mean coverage of baseline log-hazards, cumulative hazards, and transition probabilities estimated using *SSTS* and *MTS* PAMs on data simulated from *SSTS* and *MTS* DGPs.

Transition	Quantity of Interest	SSTS DGP						MTS DGP					
		SSTS PAM			MTS PAM			SSTS PAM			MTS PAM		
		Penalized Splines	Factor Smooth	(Penalized Splines, Factor Smooth)	Penalized Splines	Factor Smooth	(Penalized Splines, Factor Smooth)	Penalized Splines	Factor Smooth	(Penalized Splines, Factor Smooth)	Penalized Splines	Factor Smooth	(Penalized Splines, Factor Smooth)
0 → 1	Log-hazard	0.95 (0.93; 0.97)	0.95 (0.93; 0.97)	0.69 (0.65; 0.72)	0.68 (0.65; 0.72)	0.95 (0.93; 0.97)	0.95 (0.93; 0.97)	0.95 (0.93; 0.97)	0.95 (0.93; 0.97)	0.95 (0.93; 0.97)	0.95 (0.93; 0.97)	0.95 (0.93; 0.96)	
0 → 1	Cumulative Hazard	1.00 (0.99; 1.00)	1.00 (0.99; 1.00)	0.97 (0.95; 0.98)	0.97 (0.95; 0.98)	0.99 (0.98; 1.00)	0.99 (0.98; 1.00)	0.99 (0.98; 1.00)	0.99 (0.98; 1.00)	0.99 (0.98; 1.00)	0.99 (0.98; 1.00)	0.99 (0.98; 1.00)	
0 → 1	Transition Probability	0.91 (0.88; 0.93)	0.90 (0.88; 0.93)	0.81 (0.77; 0.84)	0.81 (0.77; 0.84)	0.90 (0.87; 0.93)	0.90 (0.87; 0.93)	0.90 (0.88; 0.93)	0.90 (0.87; 0.92)	0.90 (0.87; 0.92)	0.90 (0.87; 0.92)	0.90 (0.87; 0.92)	
0 → 3	Log-hazard	0.95 (0.93; 0.97)	0.95 (0.93; 0.97)	0.86 (0.83; 0.88)	0.87 (0.84; 0.89)	0.95 (0.93; 0.97)	0.95 (0.93; 0.97)	0.95 (0.93; 0.97)	0.95 (0.93; 0.97)	0.95 (0.93; 0.97)	0.95 (0.93; 0.96)	0.95 (0.93; 0.96)	
0 → 3	Cumulative Hazard	0.99 (0.98; 1.00)	0.99 (0.98; 1.00)	0.97 (0.96; 0.98)	0.97 (0.96; 0.98)	0.99 (0.98; 0.99)	0.99 (0.98; 0.99)	0.99 (0.98; 0.99)	0.99 (0.98; 0.99)	0.99 (0.98; 0.99)	0.99 (0.98; 0.99)	0.99 (0.98; 0.99)	
0 → 3	Transition Probability	0.91 (0.89; 0.94)	0.92 (0.89; 0.94)	0.87 (0.84; 0.89)	0.86 (0.83; 0.89)	0.92 (0.89; 0.94)	0.92 (0.89; 0.94)	0.92 (0.89; 0.94)	0.92 (0.89; 0.94)	0.92 (0.89; 0.94)	0.92 (0.89; 0.94)	0.92 (0.89; 0.94)	
1 → 2	Log-hazard	0.95 (0.93; 0.97)	0.96 (0.94; 0.97)	0.54 (0.51; 0.57)	0.54 (0.51; 0.57)	0.96 (0.94; 0.97)	0.96 (0.94; 0.97)	0.96 (0.94; 0.97)	0.96 (0.94; 0.97)	0.96 (0.94; 0.97)	0.96 (0.94; 0.97)	0.94 (0.91; 0.96)	
1 → 2	Cumulative Hazard	0.96 (0.94; 0.98)	0.97 (0.95; 0.98)	0.70 (0.67; 0.72)	0.70 (0.68; 0.72)	0.98 (0.96; 0.99)	0.98 (0.96; 0.99)	0.96 (0.95; 0.97)	0.96 (0.95; 0.97)	0.96 (0.95; 0.98)	0.96 (0.93; 0.97)	0.95 (0.93; 0.97)	
1 → 2	Transition Probability	0.93 (0.91; 0.95)	0.95 (0.92; 0.96)	0.70 (0.67; 0.73)	0.70 (0.67; 0.73)	0.94 (0.92; 0.96)	0.94 (0.92; 0.96)	0.94 (0.91; 0.95)	0.94 (0.91; 0.95)	0.93 (0.91; 0.95)	0.93 (0.91; 0.95)	0.94 (0.91; 0.95)	
1 → 3	Log-hazard	0.93 (0.91; 0.95)	0.95 (0.92; 0.96)	0.63 (0.59; 0.66)	0.63 (0.60; 0.66)	0.95 (0.93; 0.97)	0.95 (0.93; 0.97)	0.97 (0.95; 0.98)	0.97 (0.95; 0.98)	0.96 (0.94; 0.97)	0.96 (0.94; 0.97)	0.97 (0.95; 0.98)	
1 → 3	Cumulative Hazard	0.95 (0.92; 0.96)	0.96 (0.94; 0.98)	0.80 (0.77; 0.82)	0.79 (0.77; 0.82)	0.97 (0.96; 0.98)	0.97 (0.96; 0.98)	0.98 (0.97; 0.99)	0.98 (0.97; 0.99)	0.98 (0.96; 0.99)	0.98 (0.96; 0.99)	0.98 (0.96; 0.99)	
1 → 3	Transition Probability	0.91 (0.88; 0.94)	0.94 (0.91; 0.96)	0.79 (0.75; 0.82)	0.80 (0.77; 0.82)	0.94 (0.92; 0.96)	0.94 (0.92; 0.96)	0.95 (0.93; 0.97)	0.95 (0.93; 0.97)	0.94 (0.91; 0.96)	0.94 (0.91; 0.96)	0.95 (0.93; 0.97)	

Table A.3: Mean coverage of fixed effect log-hazards estimated using *SSTS* and *MTS* PAMs on data simulated from *SSTS* and *MTS* DGPs.

Transition	SSTS DGP						MTS DGP					
	SSTS PAM			MTS PAM			SSTS PAM			MTS PAM		
	Penalized Splines	Factor Smooth		Penalized Splines	Factor Smooth		Penalized Splines	Factor Smooth		Penalized Splines	Factor Smooth	
$\beta_{x_{1,0} \rightarrow 1}$	0.97 (0.95; 0.98)	0.95 (0.93; 0.97)		0.95 (0.93; 0.97)	0.95 (0.93; 0.97)		0.94 (0.92; 0.96)	0.95 (0.93; 0.97)		0.97 (0.95; 0.98)	0.95 (0.93; 0.97)	
$\beta_{x_{1,0} \rightarrow 3}$	0.99 (0.98; 1.00)	0.99 (0.98; 1.00)		0.99 (0.98; 1.00)	0.99 (0.98; 1.00)		1.00 (0.99; 1.00)	0.99 (0.98; 1.00)		1.00 (0.99; 1.00)	1.00 (0.99; 1.00)	
$\beta_{x_{1,1} \rightarrow 2}$	0.97 (0.95; 0.98)	0.98 (0.96; 0.99)		0.95 (0.92; 0.97)	0.95 (0.93; 0.97)		0.97 (0.96; 0.99)	0.99 (0.97; 0.99)		0.98 (0.97; 0.99)	0.98 (0.96; 0.99)	
$\beta_{x_{1,1} \rightarrow 3}$	0.96 (0.94; 0.98)	0.98 (0.96; 0.99)		0.95 (0.93; 0.97)	0.96 (0.94; 0.98)		0.98 (0.97; 0.99)	0.99 (0.98; 1.00)		0.98 (0.96; 0.99)	0.98 (0.95; 0.98)	

Table A.4: Details on effect sizes of risk factors for index event bias simulations. The setup for index event bias simulations is based on the simulations in Section 4.1, in particular Equations (8) and (9). The only difference now is that two risk factors x_1 and x_2 are incorporated into the log-hazard of the respective DGP (identical for *SSTS* and *MTS* DGP). This table provides details on the corresponding fixed effect sizes.

Coefficient	Effect Sizes		
	Small	Medium	Large
Transition-specific intercepts			
$\beta_{x_0,0 \rightarrow 1}$	-3.9	-3.9	-3.9
$\beta_{x_0,0 \rightarrow 3}$	-4.0	-4.0	-4.0
$\beta_{x_0,1 \rightarrow 2}$	-3.4	-3.4	-4.4
$\beta_{x_0,1 \rightarrow 3}$	-3.4	-3.4	-3.4
Transition-specific effect sizes of risk factor x_1			
$\beta_{x_1,0 \rightarrow 1}$	0.2	0.4	0.6
$\beta_{x_1,0 \rightarrow 3}$	0.0	0.0	0.0
$\beta_{x_1,1 \rightarrow 2}$	0.2	0.4	0.6
$\beta_{x_1,1 \rightarrow 3}$	0.0	0.0	0.0
Transition-specific effect sizes of risk factor x_2			
$\beta_{x_2,0 \rightarrow 1}$	0.2	0.4	0.6
$\beta_{x_2,0 \rightarrow 3}$	0.0	0.0	0.0
$\beta_{x_2,1 \rightarrow 2}$	0.2	0.4	0.6
$\beta_{x_2,1 \rightarrow 3}$	0.0	0.0	0.0

Table A.5: Correlation between two independent risk factors in simulated general population and diseased subpopulation data. This table shows mean correlation and empirical 95% confidence intervals (computed across simulation runs) between two risk factors x_1 and x_2 in states 0 and 1 from simulated multi-state data using either an *SSTS* DGP or an *MTS* DGP, described in Section 4.2.1. The two risk factors are, by construction, independent in the general population (i.e., in state 0), which is why any (negative) correlation in state 1 is induced by the restriction of the population to the index event (here: transition $0 \rightarrow 1$).

Dist. x_1	Dist. x_2	Effect Sizes	STSS DGP		MTS DGP	
			State 0	State 1	State 0	State 1
Ber(0.5)	Ber(0.5)	Small	0.00 (-0.03; 0.03)	-0.00 (-0.05; 0.04)	0.00 (-0.03; 0.03)	-0.00 (-0.05; 0.04)
Ber(0.5)	Ber(0.5)	Medium	0.00 (-0.03; 0.03)	-0.01 (-0.05; 0.03)	0.00 (-0.03; 0.03)	-0.01 (-0.05; 0.03)
Ber(0.5)	Ber(0.5)	Large	-0.00 (-0.03; 0.03)	-0.03 (-0.07; 0.02)	-0.00 (-0.03; 0.02)	-0.02 (-0.07; 0.02)
Ber(0.5)	$N(0, 1)$	Small	-0.00 (-0.03; 0.03)	-0.01 (-0.05; 0.05)	0.00 (-0.03; 0.03)	-0.00 (-0.05; 0.04)
Ber(0.5)	$N(0, 1)$	Medium	-0.00 (-0.03; 0.03)	-0.02 (-0.06; 0.03)	0.00 (-0.03; 0.03)	-0.02 (-0.06; 0.03)
Ber(0.5)	$N(0, 1)$	Large	-0.00 (-0.03; 0.03)	-0.05 (-0.09; -0.01)	0.00 (-0.03; 0.03)	-0.04 (-0.09; 0.00)
$N(0, 1)$	Ber(0.5)	Small	-0.00 (-0.03; 0.03)	-0.01 (-0.05; 0.04)	-0.00 (-0.03; 0.03)	-0.00 (-0.06; 0.04)
$N(0, 1)$	Ber(0.5)	Medium	0.00 (-0.03; 0.03)	-0.02 (-0.07; 0.03)	0.00 (-0.03; 0.03)	-0.02 (-0.07; 0.03)
$N(0, 1)$	Ber(0.5)	Large	0.00 (-0.03; 0.03)	-0.04 (-0.09; -0.00)	0.00 (-0.03; 0.03)	-0.04 (-0.09; 0.00)
$N(0, 1)$	$N(0, 1)$	Small	-0.00 (-0.03; 0.03)	-0.01 (-0.06; 0.04)	0.00 (-0.03; 0.03)	-0.01 (-0.06; 0.04)
$N(0, 1)$	$N(0, 1)$	Medium	-0.00 (-0.03; 0.03)	-0.04 (-0.09; 0.01)	0.00 (-0.03; 0.03)	-0.04 (-0.09; 0.01)
$N(0, 1)$	$N(0, 1)$	Large	-0.00 (-0.03; 0.03)	-0.08 (-0.13; -0.03)	0.00 (-0.03; 0.03)	-0.08 (-0.12; -0.03)

Table A.6: Mean coverage of baseline log-hazards under interval-censoring. This table shows mean baseline log-hazard coverage for the IC simulation settings described in Section 4.3.1. Mean coverage (95% CIs from exact binomial test) are computed pointwise across all simulation runs, then averaged over time points.

Model	Estimation Time Point	Piecewise Exponential DGP				Weibull DGP				icenReg DGP	
		Beta	Uniform	Equidistant	Beta	Uniform	Equidistant	Beta	Uniform	Equidistant	Uniform
PAM	Exact	0.94 (0.91; 0.96)	0.94 (0.91; 0.95)	0.93 (0.91; 0.95)	0.91 (0.88; 0.93)	0.90 (0.87; 0.92)	0.90 (0.87; 0.92)	0.91 (0.88; 0.93)	0.90 (0.87; 0.92)	0.90 (0.87; 0.92)	0.95 (0.86; 0.96)
PAM	Mid	0.72 (0.68; 0.75)	0.64 (0.60; 0.68)	0.55 (0.51; 0.59)	0.75 (0.71; 0.78)	0.66 (0.62; 0.70)	0.50 (0.46; 0.53)	0.75 (0.71; 0.78)	0.66 (0.62; 0.70)	0.50 (0.46; 0.53)	0.71 (0.65; 0.73)
PAM	End	0.15 (0.14; 0.17)	0.09 (0.07; 0.10)	0.54 (0.51; 0.57)	0.39 (0.36; 0.42)	0.43 (0.41; 0.45)	0.36 (0.33; 0.39)	0.39 (0.36; 0.42)	0.43 (0.41; 0.45)	0.36 (0.33; 0.39)	0.43 (0.41; 0.45)
Gen. Gamma AFT	Exact	0.11 (0.11; 0.13)	0.11 (0.11; 0.13)	0.11 (0.10; 0.13)	0.94 (0.92; 0.96)	0.93 (0.91; 0.95)	0.93 (0.91; 0.95)	0.94 (0.92; 0.96)	0.93 (0.91; 0.95)	0.93 (0.91; 0.95)	0.96 (0.89; 0.98)
Weibull AFT	Exact	0.08 (0.07; 0.09)	0.08 (0.07; 0.09)	0.08 (0.07; 0.09)	0.95 (0.93; 0.97)	0.94 (0.92; 0.96)	0.94 (0.91; 0.96)	0.95 (0.93; 0.97)	0.94 (0.92; 0.96)	0.94 (0.91; 0.96)	0.92 (0.84; 0.96)
Gen. Gamma AFT	Adjustment	0.16 (0.14; 0.18)	0.16 (0.14; 0.17)	0.13 (0.12; 0.15)	0.92 (0.90; 0.95)	0.94 (0.91; 0.95)	0.93 (0.91; 0.95)	0.92 (0.90; 0.95)	0.94 (0.91; 0.95)	0.93 (0.91; 0.95)	0.97 (0.94; 0.98)
Weibull AFT	Adjustment	0.09 (0.09; 0.11)	0.09 (0.09; 0.11)	0.08 (0.07; 0.09)	0.95 (0.93; 0.97)	0.95 (0.93; 0.97)	0.94 (0.91; 0.96)	0.95 (0.93; 0.97)	0.95 (0.93; 0.97)	0.94 (0.91; 0.96)	0.95 (0.92; 0.97)
Gen. Gamma AFT	Mid	0.13 (0.12; 0.14)	0.13 (0.12; 0.15)	0.13 (0.12; 0.14)	0.68 (0.64; 0.71)	0.76 (0.72; 0.79)	0.75 (0.71; 0.78)	0.68 (0.64; 0.71)	0.76 (0.72; 0.79)	0.75 (0.71; 0.78)	0.37 (0.34; 0.46)
Weibull AFT	Mid	0.11 (0.11; 0.13)	0.12 (0.11; 0.13)	0.09 (0.08; 0.10)	0.43 (0.40; 0.47)	0.37 (0.34; 0.41)	0.84 (0.81; 0.87)	0.43 (0.40; 0.47)	0.37 (0.34; 0.41)	0.84 (0.81; 0.87)	0.33 (0.25; 0.41)
Gen. Gamma AFT	End	0.09 (0.08; 0.11)	0.08 (0.07; 0.09)	0.14 (0.13; 0.16)	0.34 (0.31; 0.37)	0.46 (0.43; 0.48)	0.69 (0.66; 0.72)	0.34 (0.31; 0.37)	0.46 (0.43; 0.48)	0.69 (0.66; 0.72)	0.42 (0.40; 0.44)
Weibull AFT	End	0.11 (0.10; 0.12)	0.09 (0.08; 0.10)	0.15 (0.14; 0.16)	0.18 (0.16; 0.19)	0.17 (0.15; 0.18)	0.51 (0.48; 0.54)	0.18 (0.16; 0.19)	0.17 (0.15; 0.18)	0.51 (0.48; 0.54)	0.21 (0.18; 0.23)

Table A.7: Mean coverage of baseline cumulative hazards under interval-censoring. This table shows mean baseline cumulative hazard coverage for the IC simulation settings described in Section 4.3.1. Mean coverage and 95% CIs (from an exact binomial test) are computed pointwise across all simulation runs and then averaged over time points.

Model	Estimation Time Point	Piecewise Exponential DGP			Weibull DGP			icenReg DGP		
		Beta	Uniform	Equidistant	Beta	Uniform	Equidistant	Uniform	Equidistant	Uniform
PAM	Exact	0.99 (0.98; 0.99)	0.99 (0.98; 1.00)	0.99 (0.98; 0.99)	0.94 (0.92; 0.95)	0.93 (0.91; 0.95)	0.93 (0.92; 0.95)	0.98 (0.90; 0.99)		
PAM	Mid	0.92 (0.90; 0.93)	0.94 (0.92; 0.95)	0.97 (0.96; 0.98)	0.95 (0.92; 0.96)	0.89 (0.86; 0.91)	0.95 (0.93; 0.96)	0.83 (0.78; 0.84)		
PAM	End	0.45 (0.44; 0.46)	0.43 (0.42; 0.44)	0.78 (0.75; 0.79)	0.41 (0.39; 0.42)	0.36 (0.34; 0.38)	0.95 (0.93; 0.97)	0.16 (0.15; 0.18)		
Cox	Exact	0.95 (0.92; 0.96)	0.93 (0.90; 0.95)	0.94 (0.92; 0.96)	0.95 (0.92; 0.96)	0.94 (0.92; 0.96)	0.94 (0.91; 0.96)	0.76 (0.72; 0.83)		
Cox	Mid	0.77 (0.73; 0.80)	0.79 (0.76; 0.83)	0.65 (0.62; 0.68)	0.74 (0.70; 0.77)	0.75 (0.71; 0.78)	0.60 (0.56; 0.64)	0.46 (0.42; 0.54)		
Cox	End	0.36 (0.35; 0.38)	0.33 (0.31; 0.35)	0.91 (0.88; 0.93)	0.31 (0.29; 0.33)	0.20 (0.19; 0.22)	0.90 (0.88; 0.92)	0.01 (0.01; 0.02)		
Gen. Gamma AFT	Exact	0.52 (0.49; 0.55)	0.52 (0.49; 0.55)	0.52 (0.49; 0.55)	0.97 (0.96; 0.99)	0.97 (0.95; 0.98)	0.97 (0.95; 0.98)	0.99 (0.93; 1.00)		
Weibull AFT	Exact	0.36 (0.34; 0.38)	0.36 (0.35; 0.38)	0.36 (0.34; 0.38)	0.97 (0.96; 0.98)	0.96 (0.95; 0.98)	0.97 (0.95; 0.98)	0.95 (0.87; 0.98)		
Gen. Gamma AFT	Adjustment	0.80 (0.77; 0.82)	0.80 (0.78; 0.82)	0.69 (0.66; 0.72)	0.98 (0.96; 0.99)	0.98 (0.96; 0.99)	0.97 (0.95; 0.98)	0.99 (0.98; 1.00)		
Weibull AFT	Adjustment	0.50 (0.48; 0.53)	0.49 (0.46; 0.52)	0.36 (0.34; 0.38)	0.98 (0.96; 0.99)	0.97 (0.95; 0.98)	0.96 (0.94; 0.98)	0.98 (0.96; 0.99)		
Gen. Gamma AFT	Mid	0.63 (0.60; 0.66)	0.66 (0.62; 0.69)	0.61 (0.58; 0.64)	0.82 (0.79; 0.86)	0.85 (0.82; 0.88)	0.79 (0.76; 0.82)	0.48 (0.44; 0.57)		
Weibull AFT	Mid	0.46 (0.44; 0.49)	0.46 (0.43; 0.49)	0.39 (0.37; 0.41)	0.72 (0.69; 0.75)	0.67 (0.63; 0.71)	0.94 (0.92; 0.96)	0.53 (0.45; 0.59)		
Gen. Gamma AFT	End	0.27 (0.26; 0.29)	0.28 (0.27; 0.30)	0.51 (0.49; 0.53)	0.35 (0.33; 0.37)	0.25 (0.24; 0.27)	0.51 (0.48; 0.55)	0.05 (0.04; 0.07)		
Weibull AFT	End	0.19 (0.18; 0.21)	0.18 (0.17; 0.20)	0.48 (0.46; 0.50)	0.31 (0.30; 0.33)	0.29 (0.28; 0.30)	0.41 (0.38; 0.43)	0.14 (0.12; 0.16)		

Table A.8: Mean coverage of baseline survival functions under interval-censoring. This table shows mean baseline survival function coverage for the IC simulation settings described in Section 4.3.1. Mean coverage and 95% CIs (from an exact binomial test) are computed pointwise across all simulation runs and then averaged over time points.

Model	Estimation Time Point	Piecewise Exponential DGP			Weibull DGP			icenReg DGP		
		Beta	Uniform	Equidistant	Beta	Uniform	Equidistant	Uniform	Equidistant	Uniform
PAM	Exact	0.99 (0.98; 0.99)	0.99 (0.98; 1.00)	0.99 (0.98; 0.99)	0.94 (0.92; 0.95)	0.93 (0.91; 0.95)	0.93 (0.92; 0.95)	0.98 (0.90; 0.99)	0.93 (0.92; 0.95)	0.98 (0.90; 0.99)
PAM	Mid	0.92 (0.90; 0.93)	0.94 (0.92; 0.95)	0.97 (0.96; 0.98)	0.95 (0.92; 0.96)	0.89 (0.86; 0.91)	0.95 (0.93; 0.96)	0.83 (0.78; 0.84)	0.95 (0.93; 0.96)	0.83 (0.78; 0.84)
PAM	End	0.45 (0.44; 0.46)	0.43 (0.42; 0.44)	0.78 (0.75; 0.79)	0.41 (0.39; 0.42)	0.36 (0.34; 0.38)	0.95 (0.93; 0.97)	0.16 (0.15; 0.18)	0.95 (0.93; 0.97)	0.16 (0.15; 0.18)
Cox	Exact	0.95 (0.92; 0.96)	0.93 (0.90; 0.95)	0.94 (0.92; 0.96)	0.95 (0.92; 0.96)	0.94 (0.92; 0.96)	0.94 (0.91; 0.96)	0.76 (0.72; 0.83)	0.94 (0.91; 0.96)	0.76 (0.72; 0.83)
Cox	Mid	0.77 (0.73; 0.80)	0.79 (0.76; 0.83)	0.65 (0.62; 0.68)	0.74 (0.70; 0.77)	0.75 (0.71; 0.78)	0.60 (0.56; 0.64)	0.46 (0.42; 0.54)	0.60 (0.56; 0.64)	0.46 (0.42; 0.54)
Cox	End	0.36 (0.35; 0.38)	0.33 (0.31; 0.35)	0.91 (0.88; 0.93)	0.31 (0.29; 0.33)	0.20 (0.19; 0.22)	0.90 (0.88; 0.92)	0.01 (0.01; 0.02)	0.90 (0.88; 0.92)	0.01 (0.01; 0.02)
Gen. Gamma AFT	Exact	0.52 (0.49; 0.55)	0.52 (0.49; 0.55)	0.52 (0.49; 0.55)	0.97 (0.96; 0.99)	0.97 (0.95; 0.98)	0.97 (0.95; 0.98)	0.99 (0.93; 1.00)	0.97 (0.95; 0.98)	0.99 (0.93; 1.00)
Weibull AFT	Exact	0.36 (0.34; 0.38)	0.36 (0.35; 0.38)	0.36 (0.34; 0.38)	0.97 (0.96; 0.98)	0.96 (0.95; 0.98)	0.97 (0.95; 0.98)	0.95 (0.87; 0.98)	0.97 (0.95; 0.98)	0.95 (0.87; 0.98)
Gen. Gamma AFT	Adjustment	0.80 (0.77; 0.82)	0.80 (0.78; 0.82)	0.69 (0.66; 0.72)	0.98 (0.96; 0.99)	0.98 (0.96; 0.99)	0.97 (0.95; 0.98)	0.99 (0.98; 1.00)	0.97 (0.95; 0.98)	0.99 (0.98; 1.00)
Weibull AFT	Adjustment	0.50 (0.48; 0.53)	0.49 (0.46; 0.52)	0.36 (0.34; 0.38)	0.98 (0.96; 0.99)	0.97 (0.95; 0.98)	0.96 (0.94; 0.98)	0.98 (0.96; 0.99)	0.96 (0.94; 0.98)	0.98 (0.96; 0.99)
Gen. Gamma AFT	Mid	0.63 (0.60; 0.66)	0.66 (0.62; 0.69)	0.61 (0.58; 0.64)	0.82 (0.79; 0.86)	0.85 (0.82; 0.88)	0.79 (0.76; 0.82)	0.48 (0.44; 0.57)	0.79 (0.76; 0.82)	0.48 (0.44; 0.57)
Weibull AFT	Mid	0.46 (0.44; 0.49)	0.46 (0.43; 0.49)	0.39 (0.37; 0.41)	0.72 (0.69; 0.75)	0.67 (0.63; 0.71)	0.94 (0.92; 0.96)	0.53 (0.45; 0.59)	0.94 (0.92; 0.96)	0.53 (0.45; 0.59)
Gen. Gamma AFT	End	0.27 (0.26; 0.29)	0.28 (0.27; 0.30)	0.51 (0.49; 0.53)	0.35 (0.33; 0.37)	0.25 (0.24; 0.27)	0.51 (0.48; 0.55)	0.05 (0.04; 0.07)	0.51 (0.48; 0.55)	0.05 (0.04; 0.07)
Weibull AFT	End	0.19 (0.18; 0.21)	0.18 (0.17; 0.20)	0.48 (0.46; 0.50)	0.31 (0.30; 0.33)	0.29 (0.28; 0.30)	0.41 (0.38; 0.43)	0.14 (0.12; 0.16)	0.41 (0.38; 0.43)	0.14 (0.12; 0.16)

Table A.9: Mean bias of fixed effect parameter estimates under interval-censoring. This table shows the mean bias (across simulation runs) in estimating the fixed effect coefficient β_{x_1} of a *Bernoulli*(0.5)-distributed covariate x_1 for three models and three to four estimation points on data generated from two DGPs with three IC mechanisms each, described in Section 4.3.1.

Model	Estimation Time Point	Piecewise Exponential DGP			Weibull DGP		
		Beta	Uniform	Equidistant	Beta	Uniform	Equidistant
PAM	Exact	0.00	0.00	0.01	-0.01	-0.00	0.00
PAM	Mid	-0.01	0.01	0.01	0.00	0.01	-0.00
PAM	End	0.02	0.03	-0.01	0.00	0.01	-0.00
Cox	Exact	0.02	0.01	-0.01	0.01	0.00	-0.00
Cox	Mid	0.01	0.00	-0.01	0.01	0.01	-0.00
Cox	End	-0.00	0.01	-0.00	0.02	0.02	0.00
Weibull AFT	Exact	-0.04	-0.06	-0.02	-0.00	-0.00	0.00
Weibull AFT	Adj.	-0.03	-0.04	-0.05	0.00	0.00	-0.01
Weibull AFT	Mid	-0.02	-0.03	-0.04	0.02	0.02	0.03
Weibull AFT	End	-0.01	-0.01	-0.03	0.00	0.00	-0.01

Table A.10: Mean coverage of fixed effect parameter estimates under interval-censoring. This table shows mean coverage (across simulation runs) along with 95% confidence intervals (using an exact Binomial tests) of the true fixed effect parameter β_{x_1} of a *Bernoulli*(0.5)-distributed covariate x_1 for three models and three to four estimation points on data generated from two DGPs with three IC mechanisms each, described in Section 4.3.1.

Model	Estimation Time Point	Piecewise Exponential DGP			Weibull DGP		
		Beta	Uniform	Equidistant	Beta	Uniform	Equidistant
PAM	Exact	0.93 (0.91; 0.95)	0.96 (0.94; 0.97)	0.95 (0.93; 0.97)	0.98 (0.96; 0.99)	0.95 (0.93; 0.97)	0.96 (0.94; 0.98)
PAM	Mid	0.96 (0.94; 0.98)	0.95 (0.93; 0.97)	0.94 (0.91; 0.96)	0.93 (0.91; 0.95)	0.96 (0.94; 0.98)	0.95 (0.93; 0.97)
PAM	End	0.96 (0.93; 0.97)	0.95 (0.93; 0.97)	0.95 (0.93; 0.97)	0.96 (0.94; 0.97)	0.94 (0.91; 0.96)	0.95 (0.93; 0.97)
Cox	Exact	0.97 (0.95; 0.98)	0.95 (0.93; 0.97)	0.94 (0.92; 0.96)	0.94 (0.92; 0.96)	0.96 (0.94; 0.98)	0.96 (0.93; 0.97)
Cox	Mid	0.95 (0.93; 0.97)	0.96 (0.93; 0.97)	0.96 (0.94; 0.97)	0.96 (0.94; 0.97)	0.96 (0.94; 0.97)	0.94 (0.92; 0.96)
Cox	End	0.95 (0.92; 0.96)	0.95 (0.93; 0.97)	0.95 (0.92; 0.96)	0.96 (0.93; 0.97)	0.97 (0.95; 0.98)	0.95 (0.92; 0.96)
Weibull AFT	Exact	0.92 (0.89; 0.94)	0.94 (0.91; 0.96)	0.94 (0.92; 0.96)	0.95 (0.93; 0.97)	0.96 (0.94; 0.97)	0.97 (0.95; 0.98)
Weibull AFT	Adj.	0.95 (0.93; 0.97)	0.95 (0.92; 0.96)	0.93 (0.90; 0.95)	0.94 (0.92; 0.96)	0.95 (0.92; 0.96)	0.93 (0.91; 0.95)
Weibull AFT	Mid	0.92 (0.89; 0.94)	0.93 (0.90; 0.95)	0.94 (0.92; 0.96)	0.95 (0.92; 0.96)	0.96 (0.93; 0.97)	0.96 (0.94; 0.97)
Weibull AFT	End	0.95 (0.93; 0.97)	0.95 (0.93; 0.97)	0.94 (0.92; 0.96)	0.95 (0.93; 0.97)	0.96 (0.94; 0.97)	0.94 (0.92; 0.96)

Table A.11: Summary statistics of risk factors by state and rs77924615 genotype in UK Biobank. This table provides summary statistics for the six risk factors of CKD onset and progression introduced in Section 5.3.2 (median (min-max) for quantitative, n (%) for binary). For each risk factor, rows correspond to the from-state (0: Healthy; 1: Mild CKD; 2: Severe CKD; see Figure 1). The three columns correspond to the different genotypes of the genetic variant rs77924615 residing in the *UMOD* locus with effect allele G.

Risk Factor	State	Genotype of rs77924615			Total (n=130,721)
		AA (n=4,938)	AG/GA (n=40,852)	GG (n=84,931)	
Sex (Women)	0	2,554 (53.3%)	21,003 (53.5%)	43,076 (53.4%)	66,633 (53.4%)
	1	56 (43.4%)	791 (52.8%)	2,110 (52.0%)	2,957 (52.0%)
	2	7 (50.0%)	46 (47.4%)	98 (41.7%)	151 (43.6%)
PGS	0	580 (423-860)	580 (426-883)	582 (417-884)	581 (417-884)
	1	574 (465-776)	586 (443-889)	587 (444-850)	586 (443-889)
	2	572 (494-776)	580 (455-791)	582 (461-848)	580 (455-848)
Diabetes	0	386 (8.1%)	3,042 (7.7%)	6,135 (7.6%)	9,563 (7.7%)
	1	25 (19.4%)	291 (19.4%)	773 (19.0%)	1,089 (19.1%)
	2	6 (42.9%)	26 (26.8%)	67 (28.5%)	99 (28.6%)
Smoking	0	522 (10.9%)	3,944 (10.0%)	8,193 (10.2%)	12,659 (10.2%)
	1	16 (12.4%)	151 (10.1%)	404 (9.9%)	571 (10.0%)
	2	0 (0.0%)	15 (15.5%)	27 (11.5%)	42 (12.1%)
BMI	0	27.2 (16.5-55.0)	27.0 (14.3-67.3)	26.9 (12.6-74.7)	27.0 (12.6-74.7)
	1	29.0 (20.4-45.2)	28.9 (17.8-66.2)	28.8 (17.6-58.4)	28.8 (17.6-66.2)
	2	30.2 (20.9-39.9)	28.2 (18.4-48.8)	29.9 (18.3-48.3)	29.6 (18.3-48.8)
uACR	0	10.0 (2.3-1859.2)	9.8 (1.7-2918.6)	9.8 (1.7-8531.1)	9.8 (1.7-8531.1)
	1	11.4 (3.0-1611.7)	11.5 (2.4-2918.6)	10.9 (2.0-8531.1)	11.1 (2.0-8531.1)
	2	78.1 (5.2-1611.7)	25.4 (3.3-2897.2)	26.6 (3.4-8531.1)	26.6 (3.3-8531.1)
n	0	4,795 (97.1%)	39,256 (96.1%)	80,635 (94.9%)	124,686 (95.4%)
	1	129 (2.6%)	1,499 (3.7%)	4,061 (4.8%)	5,689 (4.4%)
	2	14 (0.3%)	97 (0.2%)	235 (0.3%)	346 (0.3%)

Table A.12: Comparison of genetic effect size estimates under adjustment versus weighting approaches in UK Biobank. This table compares effect size estimates of the genetic variant rs77924615 on CKD onset and progression in the UK Biobank dataset introduced in Section 5.1, using *SSTS* PAMs as introduced in Section 5.2, for four different scenarios of how to account for confounding risk factors: via direct adjustment in the model formula (Adjustment yes/no) and/or via a weighting approach using propensity scores from a multinomial logistic regression (see Appendix A.2.1). Both approaches use all risk factors introduced in Section 5.3.2.

Adjustment	Weighting	Transition	Coefficient	SE	P.value
no	no	0 → 1	0.284	0.025	<0.001
no	no	1 → 2	-0.121	0.090	0.181
no	no	2 → 3	-0.311	0.146	0.034
yes	no	0 → 1	0.278	0.026	<0.001
yes	no	1 → 2	0.045	0.100	0.654
yes	no	2 → 3	-0.159	0.178	0.371
no	yes	0 → 1	0.280	0.026	<0.001
no	yes	1 → 2	-0.049	0.101	0.627
no	yes	2 → 3	-0.134	0.179	0.454
yes	yes	0 → 1	0.277	0.026	<0.001
yes	yes	1 → 2	0.028	0.101	0.784
yes	yes	2 → 3	-0.169	0.179	0.346

0: Healthy; 1: Mild CKD; 2: Severe CKD; 3: ESKD.

Table A.13: Comparison of estimation points regarding risk factor effects in UK Biobank. This table compares effect size estimates (Coef.), standard errors (SE), and P-values of the risk factors rs77924615, sex, diabetes, and smoking status for two scenarios: when the event time point is set to the interval mid-point (left) or to the interval end-point (right). Both models are fitted to the UK Biobank dataset introduced in Section 5.1, using *SSTS* PAMs as introduced in Section 5.2.

Transition	Mid-Point Estimation			End-Point Estimation		
	Coef.	SE	P-value	Coef.	SE	P-value
G						
0→1	0.278	0.026	<0.001	0.278	0.026	<0.001
1→2	0.045	0.100	0.654	0.005	0.099	0.959
2→3	-0.159	0.178	0.371	-0.123	0.192	0.522
Sex (Women)						
0→1	0.055	0.027	0.044	0.059	0.027	0.029
1→2	-0.390	0.109	<0.001	-0.358	0.109	0.001
2→3	-0.205	0.210	0.329	-0.250	0.224	0.264
Diabetes						
0→1	-0.355	0.042	<0.001	-0.361	0.042	<0.001
1→2	-0.326	0.123	0.008	-0.284	0.124	0.022
2→3	0.036	0.241	0.880	-0.037	0.257	0.886
Smoking						
0→1	0.221	0.045	<0.001	0.231	0.045	<0.001
1→2	0.172	0.157	0.273	0.113	0.162	0.485
2→3	0.358	0.293	0.222	0.222	0.325	0.495

References

- [1] Lukasz Slawomirski et al. Progress on implementing and using electronic health record systems: Developments in oecd countries as of 2021. OECD Health Working Papers, No. 160, OECD Publishing, Paris, 2023.
- [2] Elisabeth Rau, Tim Tischendorf, and Beate Mitzscherlich. Implementation of the electronic health record in the german healthcare system: an assessment of the current status and future development perspectives considering the potentials of health data utilisation by representatives of different stakeholder groups. *Frontiers in Health Services*, 4:1370759, 2024.
- [3] Cathie Sudlow, John Gallacher, Naomi Allen, Valerie Beral, Paul Burton, John Danesh, Paul Downey, Paul Elliott, Jane Green, Martin Landray, et al. Uk biobank: an open access resource for identifying the causes of a wide range of complex diseases of middle and old age. *PLoS medicine*, 12(3):e1001779, 2015.
- [4] All of Us Research Program Investigators. The “all of us” research program. *New England Journal of Medicine*, 381(7):668–676, 2019.
- [5] KH Greiser, B Bohn, J Hilger-Kolb, L Panreck, E Breunig, W Lieb, T Pischon, T Schikowski, and H Völzke. The german national cohort (nako): Design, current state, and further follow-up data collection. *European Journal of Public Health*, 33(Supplement_2):ckad160–499, 2023.
- [6] Kidney Disease: Improving Global Outcomes (KDIGO) CKD Work Group. Kdigo 2012 clinical practice guideline for the evaluation and management of chronic kidney disease. *Kidney international supplements*, 3(1):1–150, 2013.
- [7] American Diabetes Association Professional Practice Committee. 2. diagnosis and classification of diabetes: standards of care in diabetes—2025. *Diabetes Care*, 48(Supplement_1):S27–S49, 2025.
- [8] Per K Andersen, Ornulf Borgan, Richard D Gill, and Niels Keiding. *Statistical models based on counting processes*. Springer Science & Business Media, 2012.
- [9] Richard J Cook and Jerald F Lawless. *Multistate models for the analysis of life history data*. Chapman and Hall/CRC, 2018.
- [10] Jan Beyersmann, Arthur Allignol, and Martin Schumacher. *Competing risks and multistate models with R*. Springer Science & Business Media, 2011.
- [11] Per Andersen and Niels Keiding. Multi-state models for event history analysis. *Statistical Methods in Medical Research*, 11:91–115, 05 2002.

- [12] Hein Putter, Marta Fiocco, and Ronald B. Geskus. Tutorial in biostatistics: Competing risks and multi-state models. *Statistics in Medicine*, 26(11):2389–2430, 2007.
- [13] Odd O. Aalen and Søren Johansen. An Empirical Transition Matrix for Non-Homogeneous Markov Chains Based on Censored Observations. *Scandinavian Journal of Statistics*, 5(3):141–150, 1978.
- [14] David R Cox. Regression models and life-tables. *Journal of the Royal Statistical Society: Series B (Methodological)*, 34(2):187–202, 1972.
- [15] Jonathan P Williams, Curtis B Storlie, Terry M Therneau, Clifford R Jack Jr, and Jan Hannig. A bayesian approach to multistate hidden markov models: application to dementia progression. *Journal of the American Statistical Association*, 115(529):16–31, 2020.
- [16] Yu Luo, David A Stephens, Aman Verma, and David L Buckeridge. Bayesian latent multi-state modeling for nonequidistant longitudinal electronic health records. *Biometrics*, 77(1):78–90, 2021.
- [17] Emmett B Kendall, Jonathan P Williams, Gudmund H Hermansen, Frederic Bois, and Vo Hong Thanh. Beyond time-homogeneity for continuous-time multistate markov models. *Journal of Computational and Graphical Statistics*, 34(2):668–682, 2025.
- [18] Thomas Klausch, Eddymurphy U Akwiwu, Mark A van de Wiel, Veerle MH Coupe, and Johannes Berkhof. A bayesian accelerated failure time model for interval censored three-state screening outcomes. *The Annals of Applied Statistics*, 17(2):1285–1306, 2023.
- [19] Todd Mackenzie. Survival curve estimation with dependent left truncated data using cox’s model. *The international journal of biostatistics*, 8(1), 2012.
- [20] Yu-Jen Cheng and Mei-Cheng Wang. Causal estimation using semi-parametric transformation models under prevalent sampling. *Biometrics*, 71(2):302–312, 2015.
- [21] Yuyao Wang, Andrew Ying, and Ronghui Xu. Doubly robust estimation under covariate-induced dependent left truncation. *Biometrika*, 111(3):789–808, 2024.
- [22] Simona Iacobelli and Bendix Carstensen. Multiple time scales in multi-state models. *Statistics in medicine*, 32(30):5315–5327, 2013.
- [23] Issa J Dahabreh and David M Kent. Index event bias as an explanation for the paradoxes of recurrence risk research. *Jama*, 305(8):822–823, 2011.
- [24] Zhigang Zhang and Jianguo Sun. Interval censoring. *Statistical methods in medical research*, 19(1):53–70, 2010.

- [25] Andreas Bender and Fabian Scheipl. Pammtools: Piece-wise exponential additive mixed modeling tools. *arXiv preprint arXiv:1806.01042*, 2018.
- [26] Johannes Piller, Helmut Küchenhoff, and Andreas Bender. Flexible additive models for multi-event survival analysis. In *38th International Workshop on Statistical Modelling*, page 241, 2024.
- [27] Johannes Piller, Léa Orsini, Simon Wiegrebe, John Zobolas, Lukas Burk, Sophie Hanna Langbein, Philip Studener, Markus Goeswein, and Andreas Bender. Reduction techniques for survival analysis. *arXiv preprint arXiv:2508.05715*, 2025.
- [28] Xu Zhang, Mei-Jie Zhang, and Jason P Fine. A mass redistribution algorithm for right-censored and left-truncated time to event data. *Journal of statistical planning and inference*, 139(9):3329–3339, 2009.
- [29] Edward L Korn, Barry I Graubard, and Douglas Midthune. Time-to-event analysis of longitudinal follow-up of a survey: choice of the time-scale. *American journal of epidemiology*, 145(1):72–80, 1997.
- [30] Anne CM Thiébaud and Jacques Bénichou. Choice of time-scale in cox’s model analysis of epidemiologic cohort data: a simulation study. *Statistics in medicine*, 23(24):3803–3820, 2004.
- [31] Simon Wiegrebe, Mathias Gorski, Janina M Herold, Klaus J Stark, Barbara Thorand, Christian Gieger, Carsten A Böger, Johannes Schödel, Florian Hartig, Han Chen, et al. Analyzing longitudinal trait trajectories using gwas identifies genetic variants for kidney function decline. *Nature communications*, 15(1):10061, 2024.
- [32] Bendix Carstensen Steno Diabetes Center Copenhagen. with and epi::Lexis. 2024.
- [33] Michael Friedman. Piecewise exponential models for survival data with covariates. *The Annals of Statistics*, 10(1):101–113, 1982.
- [34] Gerhard Tutz, Matthias Schmid, et al. *Modeling discrete time-to-event data*, volume 3. Springer, 2016.
- [35] Christine W. Duarte, Laura K. Vaughan, T. Mark Beasley, and Hemant K. Tiwari. Chapter 12 - multifactorial inheritance and complex diseases. In David Rimoin, Reed Pyeritz, and Bruce Korf, editors, *Emery and Rimoin’s Principles and Practice of Medical Genetics (Sixth Edition)*, pages 1–15. Academic Press, Oxford, sixth edition edition, 2013.
- [36] Mathias Gorski, Humaira Rasheed, Alexander Teumer, Laurent F Thomas, Sarah E Graham, Gardar Sveinbjornsson, Thomas W Winkler, Felix Günther, Klaus J Stark, Jin-Fang Chai, et al. Genetic loci and prioritization of genes for kidney function decline derived from a meta-analysis of 62 longitudinal genome-wide association studies. *Kidney International*, 102(3):624–639, 2022.

- [37] Jean Bretagnolle and Catherine Huber-Carol. Effects of omitting covariates in cox’s model for survival data. *Scandinavian journal of statistics*, pages 125–138, 1988.
- [38] Garrett M Fitzmaurice, Nan M Laird, and James H Ware. *Applied longitudinal analysis*. John Wiley & Sons, 2012.
- [39] Peter Diggle. *Analysis of longitudinal data*. Oxford university press, 2002.
- [40] Armend Lokku, Lily S Lim, Catherine S Birken, Eleanor M Pullenayegum, and TARGet Kids! Collaboration. Summarizing the extent of visit irregularity in longitudinal data. *BMC Medical Research Methodology*, 20:1–9, 2020.
- [41] Noorie Hyun, Li C Cheung, Qing Pan, Mark Schiffman, and Hormuzd A Katki. Flexible risk prediction models for left or interval-censored data from electronic health records. *The annals of applied statistics*, 11(2):1063, 2017.
- [42] Li C Cheung, Qing Pan, Noorie Hyun, Mark Schiffman, Barbara Fetterman, Philip E Castle, Thomas Lorey, and Hormuzd A Katki. Mixture models for undiagnosed prevalent disease and interval-censored incident disease: applications to a cohort assembled from electronic health records. *Statistics in medicine*, 36(22):3583–3595, 2017.
- [43] Matthew Sperrin, Emily Petherick, and Ellena Badrick. Informative observation in health data: association of past level and trend with time to next measurement. In *Informatics for health: connected citizen-led wellness and population health*, pages 261–265. IOS Press, 2017.
- [44] Joe Bible, Madeleine St. Ville, Paul S Albert, and Danping Liu. Accounting for informative observation process in transition models of binary longitudinal outcome: Application to medical record data. *Statistical Methods in Medical Research*, 33(2):243–255, 2024.
- [45] Audrey Boruvka and Richard J Cook. Sieve estimation in a markov illness-death process under dual censoring. *Biostatistics*, 17(2):350–363, 2016.
- [46] Patrick Schober and Thomas R Vetter. Survival analysis and interpretation of time-to-event data: the tortoise and the hare. *Anesthesia & Analgesia*, 127(3):792–798, 2018.
- [47] Andreas Bender, Andreas Groll, and Fabian Scheipl. A generalized additive model approach to time-to-event analysis. *Statistical Modelling*, 18(3-4):299–321, 2018.
- [48] Mar Rodríguez-Girondo, Thomas Kneib, Carmen Cadarso-Suárez, and Emad Abu-Assi. Model building in nonproportional hazard regression. *Statistics in medicine*, 32(30):5301–5314, 2013.

- [49] Christos Argyropoulos and Mark L Unruh. Analysis of time to event outcomes in randomized controlled trials by generalized additive models. *PloS one*, 10(4):e0123784, 2015.
- [50] Holger Sennhenn-Reulen and Thomas Kneib. Structured fusion lasso penalized multi-state models. *Statistics in Medicine*, 35(25):4637–4659, 2016.
- [51] David A Harville. Maximum likelihood approaches to variance component estimation and to related problems. *Journal of the American statistical association*, 72(358):320–338, 1977.
- [52] Ludwig Fahrmeir, Thomas Kneib, Stefan Lang, and Brian D Marx. Regression models. In *Regression: Models, methods and applications*, pages 23–84. Springer, 2022.
- [53] Simon Wood and Maintainer Simon Wood. Package ‘mgcv’. *R package version*, 1(29):729, 2015.
- [54] Takeshi Emura and Weijing Wang. Semiparametric inference for an accelerated failure time model with dependent truncation. *Annals of the Institute of Statistical Mathematics*, 68:1073–1094, 2016.
- [55] Lior Rennert and Sharon X Xie. Cox regression model under dependent truncation. *Biometrics*, 78(2):460–473, 2022.
- [56] Niklas Hagemann, Thomas Kneib, and Kathrin Möllenhoff. Capturing heterogeneous time-variation in covariate effects in non-proportional hazard regression models. *arXiv preprint arXiv:2501.13525*, 2025.
- [57] Clifford Anderson-Bergman. icenreg: regression models for interval censored data in r. *Journal of Statistical Software*, 81:1–23, 2017.
- [58] Odd Aalen. Nonparametric inference for a family of counting processes. *The Annals of Statistics*, pages 701–726, 1978.
- [59] Norman Breslow. Covariance analysis of censored survival data. *Biometrics*, pages 89–99, 1974.
- [60] Mathias Gorski, Simon Wiegerebe, Ralph Burkhardt, Merle Behr, Helmut Küchenhoff, Klaus J Stark, Carsten A Böger, and Iris M Heid. Bias-corrected serum creatinine from uk biobank electronic medical records generates an important data resource for kidney function trajectories. *Scientific Reports*, 15(1):3540, 2025.
- [61] Anna Köttgen, Cristian Pattaro, Carsten A Böger, Christian Fuchsberger, Matthias Olden, Nicole L Glazer, Afshin Parsa, Xiaoyi Gao, Qiong Yang, Albert V Smith, et al. New loci associated with kidney function and chronic kidney disease. *Nature genetics*, 42(5):376–384, 2010.

- [62] Kira J Stanzick, Klaus J Stark, Mathias Gorski, Johannes Schödel, René Krüger, Florian Kronenberg, Richard Warth, Iris M Heid, and Thomas W Winkler. Kidneygps: a user-friendly web application to help prioritize kidney function genes and variants based on evidence from genome-wide association studies. *BMC bioinformatics*, 24(1):355, 2023.
- [63] Miguel Ángel Hernán, Babette Brumback, and James M Robins. Marginal structural models to estimate the causal effect of zidovudine on the survival of hiv-positive men. *Epidemiology*, 11(5):561–570, 2000.
- [64] Miguel A Hernán, Mara McAdams, Nuala McGrath, Emilie Lanoy, and Dominique Costagliola. Observation plans in longitudinal studies with time-varying treatments. *Statistical methods in medical research*, 18(1):27–52, 2009.
- [65] Miguel A. Hernán and James M. Robins. *Causal Inference: What If*. Chapman & Hall/CRC, Boca Raton, 2020.
- [66] Olivier Devuyst and Cristian Pattaro. The umod locus: insights into the pathogenesis and prognosis of kidney disease. *Journal of the American Society of Nephrology*, 29(3):713–726, 2018.
- [67] Frank Dudbridge, Richard J Allen, Nuala A Sheehan, A Floriaan Schmidt, James C Lee, R Gisli Jenkins, Louise V Wain, Aroon D Hingorani, and Riyaz S Patel. Adjustment for index event bias in genome-wide association studies of subsequent events. *Nature communications*, 10(1):1561, 2019.
- [68] Osama Mahmoud, Frank Dudbridge, George Davey Smith, Marcus Munafò, and Kate Tilling. A robust method for collider bias correction in conditional genome-wide association studies. *Nature Communications*, 13(1):619, 2022.
- [69] Killian Donovan, Jason Torres, Doreen Zhu, William G Herrington, and Natalie Staplin. An application of the mr-horse method to reduce selection bias in genome-wide association studies of disease progression. *European Journal of Human Genetics*, pages 1–7, 2025.
- [70] Anna Fry, Thomas J Littlejohns, Cathie Sudlow, Nicola Doherty, Ligia Adamska, Tim Sprosen, Rory Collins, and Naomi E Allen. Comparison of sociodemographic and health-related characteristics of uk biobank participants with those of the general population. *American journal of epidemiology*, 186(9):1026–1034, 2017.
- [71] John Whitehead. Fitting cox’s regression model to survival data using glm. *Journal of the Royal Statistical Society Series C: Applied Statistics*, 29(3):268–275, 1980.
- [72] John D Kalbfleisch and Ross L Prentice. *The statistical analysis of failure time data*. John Wiley & Sons, 2002.